HOW DO INTRA-BASEMENT FABRICS INFLUENCE NORMAL FAULT GROWTH? INSIGHTS FROM THE TARANAKI BASIN, OFFSHORE NEW ZEALAND

Running Head: **Normal faulting influenced by basement fabrics**

Luca Collanega[1,2] *, Christopher A-L. Jackson[2], Rebecca E. Bell[2], Alexander J. Coleman[2], Antje Lenhart[2], Anna Breda[1]

[1]*Dipartimento di Geoscienze, University of Padova, Via G. Gradenigo, 6, 35131 Padova, Italy*

[2]*Basins Research Group (BRG), Department of Earth Science and Engineering, Imperial College, London, SW7 2BP, UK*

* Corresponding author: *luca.collanega@phd.unipd.it*

ABSTRACT

Pre-existing intra-basement structures can have a strong influence on the evolution of rift basins. Although 3D geometric relationships provide some insight into how intra-basement structures determine the broad geometry and spatial development (e.g. strike and dip) of rift-related faults, little is known about the impact of the former on the detailed kinematics (i.e. nucleation and tip propagation) of the latter. Understanding the kinematic as well as geometric relationship between intra-basement structures and rift-related fault networks is important, with the extension direction in many rifted provinces typically thought to lie normal to fault strike. We here investigate this problem using a borehole-constrained, 3D seismic reflection dataset from the Taranaki Basin, offshore New Zealand. Excellent imaging of intra-basement structures and a relatively weakly-deformed, stratigraphically simple sedimentary cover allow us to: (i) identify a range of interaction styles between intra-basement structures and overlying, Plio-Pleistocene rift-related normal faults; and (ii) examine the cover fault kinematics associated with each interaction style. Some of the normal faults parallel and are physically connected to intra-basement reflections, which are interpreted as mylonitic thrusts related to Mesozoic subduction and basement terrane accretion. These geometric relationships indicate pre-existing, intra-basement fabrics locally controlled the position and attitude of Plio-Pleistocene rift-related normal faults. However, through detailed 3D kinematic analysis of selected normal faults, we show that: (i) normal faults only nucleated above intra-basement structures that experienced Late Miocene compressional reactivation; (ii) thrusts and folds resulting from Late Miocene reactivation and upward propagation of intra-basement structures acted as nucleation sites for Plio-Pleistocene rift-related faults; and (iii) despite playing an important role during rifting, intra-basement structures do not appear to have been significantly extensionally reactivated. Our analysis shows how km-wide, intra-basement structures can have a temporally and spatially far-reaching influence over the nucleation and development of newly formed normal faults, principally due to local perturbation of the regional stress field. Because of this, simply inverting fault strike for causal extension direction may be incorrect, especially in provinces where pre-existing, intra-basement structures occur. We also show that a detailed kinematic analysis is key to deciphering the temporal as well as simply spatial or geometric relationship between structures developed at multiple structural levels.

1. Introduction

Crystalline basement typically hosts a variety of mechanical anisotropies consisting of structures at different scales; e.g. metamorphic mineral fabrics, brittle faults, fracture networks, ductile shear zones, and major tectonic boundaries. Pre-existing structures may control the strike and distribution of normal faults developed during rifting, resulting in the formation of non-colinear fault networks (e.g. Korme *et al.*, 2004; Morley *et al.*, 2004; Reeve *et al.*, 2015). However, non-colinear fault systems may also form in response to multiphase rifting (Duffy *et al.*, 2015), the breaching of relay zones bound by otherwise co-linear faults (e.g. Trudgill, 2002), the development of release faults (e.g. Destro, 1995), or local stress perturbation around major faults (Maerten *et al.*, 2002). Understanding the causal mechanism underlying the formation of non-colinear faults is crucial when attempting to infer and reconstruct the stresses and overall tectonic history of an area (cf. Peace *et al.*, 2017). Intra-basement structures can affect large-scale rift development, as recognized in the North Sea (e.g. Bartholomew *et al.*, 1993; Doré *et al.*, 1997; Fossen *et al.*, 2016; Phillips *et al*., 2018), the Barents Sea (e.g. Ritzmann and Faleide, 2007; Gernigon *et al.*, 2014), the East African Rift (e.g. Ring, 1994; Modisi *et al.*, 2000), and the Taranaki Basin (Muir *et al.*, 2000). Offshore-onshore correlations, combined with aeromagnetic data, suggest pre-existing basement structures can control the position of major basin-bounding fault systems, shaping the overall rift physiography (e.g. Muir *et al.*, 2000; Gernigon *et al.*, 2014; Fazlikhani *et al.*, 2017). However, at the scale of individual fault segments, the influence of intra-basement structures appears uncertain, suggesting structural inheritance may be scale-dependent (Kirkpatrick *et al.*, 2013; Reeve *et al.*, 2013; Phillips *et al*., 2016).

3D seismic reflection data allow the three-dimensional geometric relationships between intra-basement structures and normal faults to be resolved (e.g. Reeve *et al.*, 2013; Bird *et al.*, 2014; Siuda *et al.*, in review). Analysis of 3D seismic data from the North Sea show that pre-existing structures can be either reactivated or cross-cut by later normal faults, with dip and obliquity with respect to the new extension direction thought to be the key factors controlling their selective reactivation (Phillips *et al.*, 2016; Claringbould *et al.*, 2017; Fazlikhani *et al.*, 2017). However, intra-basement structures may exert their influence through other processes rather than simple reactivation, for example by acting as nucleation sites for later-formed normal faults, or by perturbing the local stress field such that faults have strikes oblique to the prevailing extension direction (Phillips *et al.*, 2016). New normal faults may nucleate preferentially in the weak regions offered by pre-existing structures, even when pre-existing structures are not directly reactivated; such examples of this spatial and kinematic relationship are shown in the physical models of Faccenna *et al.* (1995), Henza *et al.* (2010), Henza *et al.* (2011), and the numerical models of Deng *et al.*, (2017). Furthermore, local stress perturbations near pre-existing structures are supported by inversion of earthquake focal mechanisms (Morley, 2010), analysis of borehole break-out data (King *et al.*, 2010), and the outputs of numerical models (Homberg *et al.*, 1997; Maerten *et al.*, 1999; Maerten *et al.*, 2002). Recently, Duffy *et al.* (2015) highlighted the potential of three-dimensional, 3D seismic reflection-based kinematic analysis for reconstructing the evolution of complex fault interaction styles and genetic relationships. However, to the best of our knowledge, this powerful approach has not yet been applied to the interactions between intra-basement structures and overlying, rift-related normal fault networks.

In this study we: i) identify and characterise a range of three-dimensional geometric relationships between intra-basement structures and overlying normal faults; ii) use growth strata and fault displacement distribution mapping to perform a kinematic analysis of the normal faults; and iii) based on their geometric and kinematic relationships, interpret how intra-basement structures influenced the development of the rift-related normal faults. To do this we use 3D seismic reflection and well data from the western margin of the Taranaki

Basin, offshore New Zealand (Fig. 1). The shallow depth of the crystalline basement (*c.* 3.5 km) results in excellent seismic imaging of the intra-basement structures; this, combined with a stratigraphically simple, relatively low-strain setting, makes this an ideal location to examine the early-stage interactions between intra-basement structures and overlying, rift-related normal faults. We first use qualitative, plan-view- and cross-section-based observations to show that, to the first-order, intra-basement structures controlled the growth of the later, rift-related normal fault network (Bird *et al.*, 2015; Peace *et al.*, 2017). We then conduct a quantitative, three-dimensional analysis of throw distributions on individual fault surfaces to understand how each interaction style evolved (cf. Duffy *et al.*, 2015). Our 3D kinematic analysis shows how local perturbation of the regional stress field and preferential nucleation from pre-existing structures can strongly influence the development of overlying rift-related normal fault network, resulting in characteristic spatial and temporal relationships between structures at different levels.

2. Geological framework

The Taranaki Basin is situated mostly offshore the west coast of New Zealand's North Island. The basin is defined by two major, approximately N-trending fault systems: the Cape Egmont and Taranaki faults (Fig. 1). Our study area sits mostly on the footwall of the Cape Egmont Fault (Fig. 2B).

2.1. Basement geology

The basement structural grain of the Taranaki Basin developed during Mesozoic subduction and terrane accretion along the SW-Pacific margin of Gondwana (e.g. Bradshaw, 1989; Fig. 2A). By the Early Cretaceous, subduction had resulted in the juxtaposition of three approximately N-trending basement terranes (Bradshaw, 1993; Kimbrough *et al.*, 1993; Fig. 1): (i) the Western Province, consisting of a Gondwana fragment made up of mainly meta-sedimentary rocks (Bradshaw *et al.*, 1997; Mortimer *et al.*, 1997), (ii) the Eastern Province, comprising arc volcanic and arc-derived meta-sedimentary sequences (e.g. Bradshaw, 1989) and (iii) the Median Tectonic Zone, a narrow belt of plutonic rocks, which separates the Western and Eastern Provinces (e.g. Bradshaw, 1993; Mortimer *et al.*, 1999). This basement fabric influenced the subsequent structural evolution of the sedimentary cover during the Cenozoic, with the Cape Egmont and Taranaki Faults exploiting the boundaries between basement terranes (Muir *et al.*, 2000; Fig. 1).

2.2. Structural Evolution of the Southern Taranaki Basin

The Taranaki Basin developed in response to Late Cretaceous-Early Eocene and Plio-Pleistocene rifting (Fig. 2A). During the Eocene-Miocene, regional extension was punctuated by a phase of tectonic quiescence and basin inversion. The Late Cretaceous-Early Eocene rift event is related to the break-up of Gondwana, and was associated with thermally induced uplift, resulting in the development of a major regional unconformity at the top of the crystalline basement (Moore *et al.*, 1986; Strogen *et al.*, 2017). Normal faulting initiated in the Mid-Cretaceous and continued until the Paleocene, with the cessation of faulting being diachronous across the Taranaki Basin (Strogen *et al.*, 2017). This rift event formed a series of NE-trending half-graben (e.g. Maui Sub-basin, Pakawau Sub-basin, Kiwa Sub-basin) that filled with up to 1800 m of fluvial-deltaic-to-shallow marine sediments sourced from the adjacent fault scarps (North Cape and Farewell formations; King and Thrasher, 1996; Fohrmann *et al.*, 2012; Reilly *et al.*, 2015; Strogen *et al.*, 2017). Once rifting ceased, post-rift thermal subsidence resulted in an overall deepening of the basin and the deposition of mudstonedominated, marine sediments (Turi Formation; King and Thrasher, 1996; Strogen, 2011; Strogen *et al.*, 2014).

In the Mid-Eocene, in response to the onset of subduction of the Pacific Plate along the Hikurangi Trough, compression initiated across much of the Taranaki Basin (e.g. Rait *et al.*, 1991; Stagpoole and Nicol, 2008). During the Miocene, compression spread westwards from the eastern boundary of the Taranaki Basin, with inversion of the Cape Egmont Fault occurring in the late Miocene (Nicol *et al.*, 2005). Shortening was associated with the formation of NE-to-NNW-trending reverse faults and folds, which occasionally exploited pre-existing normal faults and basement fabric (Reilly *et al.*, 2015). In the Southern Taranaki Basin, compression was rapidly followed by back-arc extension at about 4 Ma, with this tectonic regime continuing to the present day (e.g. Giba *et al.*, 2010; Mouslopoulou *et al.*, 2012). The dominant strike of the Plio-Pleistocene rift-related normal faults is NE-SW, with NNE-SSW-striking normal faults prevailing west of the Cape Egmont Fault (Reilly *et al.*, 2015). This fault pattern is consistent with the current NW-SE regional extension direction indicated by borehole breakouts and focal mechanisms (Giba *et al.*, 2010). During Plio-Pleistocene rifting, reactivation and upward propagation of pre-existing, predominantly Late Cretaceous-to-Paleocene faults resulted in the formation of relatively small (in terms of displacement), N-S-striking segments (Giba *et al.*, 2012). The magnitude of Plio-Pleistocene regional extension is relatively small (stretching factor β=1.014), being largely focussed on the Cape Egmont Fault (Reilly *et al.*, 2015).

3. Dataset

We use a 1500 km^2, pre-stack time-migrated, 3D seismic reflection dataset and seven wells (Fig. 3), the latter containing well-log, formation top and biostratigraphic data. Two wells

(Maui-2 and Rahi-1) penetrate the uppermost part of the crystalline basement. The 3D survey has a record length of 5500 ms two-way time (TWT), and a vertical sampling interval of 3 ms, with an inline (N-trending) and crossline (E-trending) spacing of 25 m and 12.5 m, respectively. Seismic data are presented with SEG normal polarity, such that trough events (blue reflections) correspond to a downward decrease in acoustic impedance and peak events (red reflections) correspond to a downward increase in acoustic impedance. The dominant frequency decreases downwards from *c.* 50 Hz in the Pliocene interval (c. 750 ms TWT) to *c.* 35 Hz in the shallow crystalline basement (c. 2700 ms TWT); taking velocity data for the sedimentary cover from wells, and by assuming a velocity of 5500 ms^{-1} for the crystalline basement based on its lithologic composition (i.e. metasedimentary rock; cf. Muir *et al.*, 2000), we estimate a downward decrease of the vertical seismic resolution from *c.* 10 m to 40 m.

4. Methods

To map the plan-view distribution of the intra-basement structures we used a seismic attribute sensitive to amplitude contrast (i.e. Root Mean Square or 'RMS' amplitude attribute), and one revealing the normalized dip of the reflections (i.e. Dip Illumination). We mapped the Top Basement and eight key seismic horizons across the survey area, tying them to wells using checkshots and synthetic seismograms (Fig. 2A). To constrain the onset of rift-related faulting, we created isochron (thickness) maps between the Top Basement and the Top Farewell Formation, the Top Upper Manganui and Intra-Giant Foresets formations, and the Intra-Giant Foresets and the Top Giant Foresets formations (Fig. 2A). We compared the spatial distribution of intra-basement structures and normal faults at different stratigraphic levels, and evaluated their connectivity in cross-section, thereby revealing their three-dimensional geometric relationships.

To determine how each geometric relationship developed, we carefully reconstructed the 3D geometry of, and throw distribution on, key faults. We infer regions of high-displacement represent fault nucleation points, whereas local throw minima represent areas of fault linkage (Walsh and Watterson, 1987; Mansfield and Cartwright, 1996; Walsh *et al.*, 2003; Giba *et al.*, 2012). Throw distribution on the fault surface can thus be used to determine if the fault grew as a single, isolated structure, or whether it evolved through the coalescence of initially isolated segments. We mapped faults on seismic sections taken orthogonal to fault strike at intervals of 62.5 m, paying particular attention to tip line position and degree of linkage with intra-basement structures. We determined the footwall and hanging wall cut-offs for 8-15 horizons to constrain throw variations across the fault surface. In order to remove the effect of fault-related folding, and to thus account for the continuous (ductile) component of strain, we projected the regional trend of horizon dip away from the fault-related folds (Appendix B). We displayed throw values as throw-depth (T-z) plots, where the throw is plotted against the depth to the midpoint between hanging-wall and footwall cut-offs (e.g. Muraoka and Kamata, 1983; Cartwright *et al.*, 1995; Hongxing and Anderson, 2007; Baudon and Cartwright, 2008a, b and c). From these data we compiled fault strike-projections (e.g. Walsh and Watterson, 1991; Duffy *et al.*, 2015). Finally, we converted our TWT kinematic analysis to the depth domain using a simple best-fit second-order polynomial relationship derived from the time-depth curves of two nearby wells (Appendix C). The measurement error imposed by well-derived velocity variations increases downwards from 10 m in the Pliocene interval to 190 m immediately above Top Basement. Given the simple velocity structure of the sedimentary cover, this error may influence the absolute throw values presented, but will not significantly influence the overall throw pattern on, or kinematic interpretation of, individual segments (cf. Baudon and Cartwright, 2008c; Conneally *et al.*, 2014; Duffy *et al.*, 2015). In addition, because of: (i) the stratigraphically simple, sub-horizontally layered nature of the host rock; and (ii) the relatively low throw values, meaning footwall and hangingwall strata are not buried to significantly different depths, we argue that primary throw distribution will not be substantially altered by ongoing and/or subsequent compaction or differential compaction (cf. Mansfield and Cartwright, 1996; Taylor *et al.*, 2008).

5. Interpretation of intra-basement structures

5.1. Types of intra-basement reflections

Intra-basement reflections are well-imaged within the upper ~1000 ms TWT of the basement rocks (c. 5500 m below Top Basement). The crystalline basement is generally acoustically transparent, with sub-horizontal reflections in the upper part (Figs. 4D and E). The most prominent features in the crystalline basement are medium-to-high amplitude, continuous to semi-continuous, gently west-dipping (15° to 30°) reflections defined by a peak-trough-peak wave train (Fig. 4). Based on their amplitude, spacing, and vertical and lateral continuity, these reflections can be subdivided into three types (Figs. 4C, D and E):

- Type 1 consists of a *c.* 2.5 km-wide zone of shallowly dipping (15°-20°) reflections (Fig. 4A). The seismic character changes laterally within this package, from high-amplitude, continuous reflections at the boundaries, to chaotic, discontinuous, folded reflections towards the centre. Type 1 reflections typically offset Top Basement (Fig. 4C).
- Type 2 is represented by narrow (*c.* <100 m-wide), isolated, high-amplitude reflections that dip at 20°-30° and have a lateral spacing of 1-2 km (Fig. 4B). Reflections are vertically continuous from the Top Basement to the survey record length (5500 ms). Type 2 reflections typically offset Top Basement (Fig. 4D).

- Type 3 has similar characteristics to Type 2, but the reflections are weaker and vertically segmented (<200 m high; Fig. 4E). Type 3 reflections are truncated by the Top Basement Unconformity (Fig. 4E).

5.2. Plan-view distribution

Type 1 reflections are only observed in a broadly N-trending, 5 km-long, 2.5 km-wide zone in the northern part of the survey (Fig. 5A). The eastern and western boundaries of this zone are relatively sharp. In contrast, the southern boundary is gradational, with several Type 2 reflections splaying off from the package of Type 1 reflections (Figs. 5B and C). Type 2 and Type 3 reflections are typically 1-15 km long, curvilinear (Fig. 5C), and trend NNW to NNE (see rose diagram in Fig. 5C). Type 2 reflections are concentrated in the central part of the survey (Fig. 5C) and are laterally continuous (Fig. 5B). In contrast, Type 3 reflections occur in the eastern and western sectors (Fig. 5C), and are segmented along strike (<3 km long segments; Fig. 5B). Type 2 and Type 3 reflections are often interconnected, displaying an anastomosing geometry (Fig. 5C).

5.3. *Top Basement Structures*

The Top Basement is dominated by reverse faults and folds in the central and south-western parts of the survey, with minimal normal faulting in the east (Fig. 6B). Reverse structures are curvilinear in map-view, and are up to 15 km long, strike NNW-SSE to NNE-SSW (see upper rose diagram in Fig. 6C), and dip westwards. Of the 22 reverse displacement structures (i.e. thrusts and folds), 16 correlate with the intra-basement reflections on time-slice 2871 ms for at least some of their strike length, with 6 thrusts being physically connected to intra-basement reflections for their total strike length (Fig. 6C). In particular, the eastern boundary of the Type 1 reflections zone, and the entirety of a Type 2 reflection connected to it at its southeastern corner, are expressed by prominent anticlines and reverse faults at Top Basement level (Figs. 4C, D and 6C). By contrast, the Type 3 reflections in the eastern part of the survey, and the closely spaced Type 2 reflections in the central part of the survey, are truncated by the Top Basement Unconformity (Fig. 6C), with flat-lying reflections overlying them in the sedimentary cover (Fig. 4E). Normal faults at Top Basement level are linear and strike NE-SW to NNE-SSW (see lower rose diagram in Fig. 6C), with a maximum length of 7 km (Fig. 6B), and displacements of 25-65 ms TWT (50-125 m). They generally show no direct spatial correlation with the intra-basement reflections on time-slice 2871 ms (Fig. 6C) and three of them terminate along-strike against reverse structures (Fig. 6B). In cross-section, reverse faults have a vertical extent of 100-200 ms TWT (150-350 m), with a maximum throw of 30 ms TWT (60 m) at Top Basement (Figs. 4C and D). Reverse faults are typically overlain by west-facing monoclines (Fig. 4C) and anticlines (Fig. 4D), and are physically connected to Type 1 and Type 2 reflections (Figs. 4C and D). In some instances, reverse faults at Top Basement level may become normal faults at shallower levels (Figs. 4A and B).

5.4. Origin of intra-basement reflections

Prominent intra-basement reflections are typically interpreted as the seismic expression of mylonites within ductile shear zones (e.g. Brewer *et al.*, 1983; Wang *et al.*, 1989; Reeve *et al.*, 2013; Phillips *et al.*, 2016). In particular, the trough-peak-trough wavetrain of intra-basement reflections (Fig. 4) are interpreted as the result of the interference between stacks of 50-100 m thick layers of mylonitic and relatively undeformed rock (Fig. 4) (e.g. Fountain *et al.*, 1984; Hurich *et al.*, 1985; Reeve *et al.*, 2013; Phillips *et al.*, 2016). In addition, the anastomosing geometry of the intra-basement reflections (Fig. 5) strongly resembles the typical pattern of shear zones (e.g. Arbaret and Burg 2003; Carreras *et al.*, 2010; Rennie *et al.*, 2013). We therefore interpret the thick package of reflections (i.e. Type 1; Fig. 4C) as the seismic expression of a stack of mylonitic and intervening, relatively undeformed protolith layers (cf. Phillips *et al.*, 2016). The chaotic seismic character in the centre of the Type 1 structure (Fig. 4C) could be due to lateral variations in composition, different amounts of strain, or complex internal geometries (Klemperer, 1987; Brocher and Christensen, 1990; McDonough and Fountain, 1993; Lenhart *et al.*, in review). An alternative interpretation is that the discontinuous, complex reflections may be related to destructive interference between adjacent mylonitic bands (Phillips *et al.*, 2016). The low dip (20°-30°) of the isolated reflections (i.e. Type 2 and Type 3; Figs. 4B, D and E) suggests they may have formed as mylonite-bearing thrusts. The higher amplitude of Type 2 (Fig. 4D) compared to Type 3 (Fig. 4E) structures may reflect an increase of the acoustic impedance contrast due to the development of preferred crystallographic orientations and mineralogical segregation during mylonitization (e.g. Robin, 1979).

The erosive truncation of intra-basement structures by the Top Basement Unconformity (Fig. 4E) indicate they developed before the onset of sedimentation, and thus before the Paleocene (Fig. 2). Furthermore, the shallow dip of intra-basement structures suggests development during a phase of horizontal shortening, making Mesozoic subduction and basement terrane accretion the most likely event responsible for their origin (e.g. Muir *et al.*, 2000). This hypothesis is also supported by the strike of the intra-basement structures, which is broadly parallel to the Mesozoic basement terrane boundaries (cf. Figs. 1 and 5C). The successive kinematic history of the intra-basement structures was reconstructed based on their expression on Top Basement (Fig. 6) due to the lack of pre-kinematic markers within the basement rocks (i.e. reflective, pre-kinematic layering). The plan-view correlation and physical connection between several intra-basement structures and the Top Basement thrusts/folds (Fig. 6C) suggest compressional reactivation and upward propagation of the former (e.g. Mitra, 1990; Erslev and Mayborn, 1997; Brandes and Tanner, 2014), with vertically and laterally continuous intra-basement structures (i.e. Type 1 and 2) being preferentially reactivated. We attribute this compressional reactivation to the late Miocene inversion (e.g. Reilly *et al.*, 2015), as this is the only compressional event that affected the Taranaki Basin during the Cenozoic.

6. Structures within the sedimentary cover

6.1. Structural style

The Top Tikorangi Horizon illustrates the structural style at a distance of 350-450 ms TWT (650-850 m) above Top Basement (Fig. 2A). Here, deformation is characterised by several (n=45), low displacement (<50 m) normal faults, concentrated in a N-trending zone in the central part of the survey area (Figs. 7A and B). Most of the normal faults strike from NNE-SSW to NE-SW and dip to the west, although some strike NW-SE to N-S (Fig. 7B). The fault segments are generally 5 km long with a lateral spacing of 1-2 km in the central survey area, increasing to > 4 km in the eastern and western areas (Fig. 7B).

The Intra-Giant Foresets Formation Horizon illustrates the fault pattern at a distance of 1850-1950 ms TWT (2000-2100 m) above Top Basement (Fig. 2A). In the central-eastern part, the horizon is cross-cut by several (n=23), low-displacement (<30 m), closely-spaced (<3 km) normal faults (Figs. 7C and D). The normal faults strike from NNE-SSW to NE-SW, except for three N-S-striking fault segments in the north of the survey (F7a, b and c; Figs. 7D and E). Most of the normal faults dip to the west, being >5 km long and linear in map-view (Figs. 7C and D); only one fault is curvilinear, curving to a N-S strike in the central portion (see red box in Fig. 7D).

6.2. Timing of normal faulting

Having established the geometry of the normal fault network, we use thickness and seismic-stratigraphic patterns to deduce its temporal evolution. In particular, we describe and interpret the isochron maps of the stratigraphic intervals corresponding to the main rifting events shaping the southern Taranaki Basin (i.e. Paleocene and Pliocene intervals).

The Paleocene succession (65-55 Ma) comprises the Farewell Formation, which uncomformably overlies the crystalline basement (Fig. 2A). The isochron for the Top Basement - Top Farewell Formation interval illustrates an overall northward thickening from 40 to 170 ms TWT (c. 250 m; Fig. 8A), with localised thinning (<30 ms TWT, c. 50 m) above intra-basement structures. For example, we clearly observe thinning of this interval corresponding to the eastern boundary of the Type 1 structure (see red box in Fig. 8A). The absence of thickening into the hanging-wall of normal faults (Fig. 8A), and the lack of wedge-shaped seismic geometries (Fig. 2A) in the Top Basement - Top Farewell Formation interval (65-55 Ma), together suggest the study area was not affected by Late Cretaceous-Early Eocene rifting. This interpretation is supported by the development of conformable, flat-lying, onlapping reflections on the Top Basement (Fig. 2A), suggesting simple infill of inherited relief during the Paleocene.

The overlying Pliocene succession (5.3-2.5 Ma) comprises northward prograding clinothems of the Giant Foresets Formation (e.g. Hansen and Kamp, 2002, 2004; Chenrai and Huuse, 2017; Fig. 2A). In our study area, this succession can be split into two parts based on a vertical change in seismic facies defined by the Intra-Giant Foresets Formation horizon (Fig. 2A). The interval between the Top Upper Manganui Formation and the Intra-Giant Foresets Formation horizons (5.3-3 Ma) thickens northwards from 170 to 270 ms TWT (c. 100 m; Fig. 8B). Within this interval, minimal thickness variations have been observed across the normal faults. The interval between the Intra-Giant Foresets Formation horizon and the Top Giant Foresets

Formation (3-2.5 Ma) locally thickens (20 ms TWT, *c.* 20 m) across the NNE-SSW-striking segments (F1, F2 and F6) and the N-S striking segments (F7a-c), delineating two distinct Pliocene depocentres (Fig. 8C). These across fault thickness variations constrain the onset of faulting 3-2.5 Ma (cf. Giba *et al.*, 2010). The rapid change in the thickness pattern between the 5.3-3 Ma and 3-2.5 Ma intervals (cf. Figs. 8B and C), and the elongated shape of the depocentres (Fig. 8C) suggest the bounding normal faults relatively rapidly established their total length in <0.5 Ma.

6.3. Basement structure-cover faults plan-view relationships

In this section, we compare the structural trends immediately below (Fig. 5) and at Top Basement level (Fig. 6) with the normal faults defined at multiple structural levels in the overlying sedimentary cover (i.e. Top Tikorangi Formation, Fig. 7B; and Intra-Giant Foresets Formation horizon, Fig. 7D). Cover faults having different degrees of physical connectivity to intra-basement structures generally display different strikes and vertical extent. Nine normal faults appear physically connected to intra-basement structures for ≥ 90 % of their strike length (blue segments in Figs. 7B and D). These dominantly connected normal faults strike NNW-SSE to N-S (Fig. 7) and generally only extend <1500 m above Top Basement (cf. Figs. 7B and D). Within this group of normal faults, only the N-S-striking fault segments that are connected to the Type 1 structure (F7a-c) extend through the whole sedimentary succession and cross-cut the Intra-Giant Foresets Formation horizon (Fig. 7E). On the other hand, the majority of normal faults (36 out of 45) are physically disconnected or are connected to intra-basement structures for ≤ 50% of their strike length (brown segments in Figs. 7B and D). These partially connected/disconnected normal faults strike NE-SW to NNE-SSW (Fig. 7D) and extend up to 3000 m above Top Basement, crosscutting almost the entire cover succession (cf. Figs. 7B and D). Interestingly, the physical connection between intra-basement structures and normal faults only occurs where also the former strike NE-SW to NNE-SSW, resulting in limited twisting of the fault surface.

7. 3D geometry and throw distribution on cover normal faults

We identify four possible styles of interaction and linkage between normal faults in the sedimentary cover and intra-basement structures based on their 3D geometric relationships, and throw distribution on the former. These styles are: I) normal faults physically disconnected from intra-basement structures; II) NW-SE-striking normal faults physically connected to Type 2 structures; III) NNE-SSW-striking normal faults physically connected to Type 2 structures; and IV) N-S-striking normal faults physically connected to the Type 1 structure.

7.1. Normal faults physically disconnected from intra-basement structures

Faults F1 and F2 are representative of the NE-SW to NNE-SSW-striking normal faults that are physically disconnected from the intra-basement structures (Fig. 9E). Both F1 and F2 are linear in map view (Fig. 9E), dip westwards (Fig. 9B), and are characterised by minor, across-fault thickening of the interval between the Intra-Giant Foresets Formation and the Top Giant Foresets Formation horizons (20 ms TWT, c. 20 m; Fig. 8C). However, we note that the expansion index is c. 1 at the lateral tips of F1 and F2 (Fig. 9D), suggesting that, in these regions at least, the faults never reached the surface and remained blind. The tip line of F1 is semi-elliptical, with a flat upper tip line in the Pliocene interval, and an arcuate lower tip line in the Eocene/Miocene succession (Fig. 9A). The fault is tallest (c. 2000 m) at its centre (Fig. 9A). The throw contours on the fault surface define a “bullseye pattern”, centered on a throw maximum (*c.* 30 m) in Miocene strata. The throw gradient is higher towards the upper tip line than the lower or lateral tips (Fig. 9A). F2 is up to 2400 m tall, with a relatively irregular, concave downward, crescentic fault surface (Fig. 9A), which may reflect the strain shadowing (e.g. Gupta and Scholz, 2000) due to the flanking faults (F1 and F6; Fig. 7D). The lower tip line is c. 200-500 m above an underlying, N-trending Type 2 intra-basement structure (Figs. 9B and E) that, differently from several other Type 2 intra-basement structures, do not appear to have been significantly reactivated during the late Miocene inversion, as indicated by the absence of associated thrusts and folds at Top Basement level. T-z profile for F2 is broadly symmetrical, with a single throw maximum at the fault centre (*c.* 30 m) decreasing radially and smoothly away from this point towards the tip line (Figs. 9A and C; cf. "C-type" profiles of Muraoka and Kamata, 1983).

7.2. NW-SE-striking normal faults physically connected to Type 2 structures

Faults F3-5 represent examples of NW-SE-striking normal faults that are physically connected to Type 2 structures along most of their strike length (Fig. 10E). F3-5 are <1500 m tall, offsetting only the lowermost part of the sedimentary cover (Fig. 10B), and are not associated with any significant across-fault thickness variations (Figs. 8 and 10D). F3 is *c.* 3 km long, with its upper tip line located in Middle Miocene strata, c. 1500 m above Top Basement (Figs. 10A and B). F4 and F5 are shorter (*c.* 1 km) than F3, terminating upwards in Eocene strata, c. 800 m above Top Basement (Fig. 10A). Each fault displays a single throw maximum (*c.* 30-40 m) in Eocene strata (Fig. 10A), with throw decreasing smoothly away from this point towards its tip line (Fig. 10A). The key difference between F3-5, and normal faults physically disconnected from intra-basement structures (i.e. F1-2), is the negative (i.e. reverse) throw region (up to -30 m) just above Top Basement (cf. Figs. 9A and 10A).

7.3. NNE-SSW-striking normal faults physically connected to Type 2 structures

Fault F6 is representative of the numerous NNE-SSW-striking normal fault physically connected to Type 2 structures (Fig. 11E). F6 consists of two vertically offset, c. 5 km long segments (F6a, lower segment; and F6b, upper segment), with a total fault height of *c.* 2900 m (Fig. 11A). The lower fault segment, F6a, is physically connected to the underlying Type 2 structure along its central portion (for c. 50% of its total length; Fig. 11A) as well as to the overlying normal fault segment F6b (for c. 1 km; Fig. 11A). No across-fault thickness variations occur in association with F6a, although the Paleocene thins slightly from the fault footwall to its hangingwall (Fig. 8A; see also expansion index values <1 in Fig. 11D). The T-z plot for F6a reveals a throw maximum in Eocene strata (*c.* 60 m) and, in a similar way to F3-5, negative throw values (up to -40 m) near Top Basement (Fig. 11C). This Eocene throw maximum is elongated, approximately corresponding to the area of physical linkage between this and the underlying intra-basement structure (Fig. 11A). The upper segment F6b is associated with across-fault thickening of Pliocene strata (Fig. 8C) and a flat upper tip line (Fig. 11A). The throw maximum on F6b is located in Miocene rocks (*c.* 60 m), with the throw profile being slightly skewed towards the fault lower tip (Figs. 11A and C). Throw values are higher towards the zone of physical connection with the lower segment (F6a) than towards the tip line (Fig. 11A).

7.4. N-S-striking normal faults physically connected to the Type 1 structure

Fault F7 represents the normal faults physically connected to the Type 1 structure, which is located in the northern part of the study area (Figs. 12B and E). F7 is at least *c.* 5 km long and 3200 m tall (Fig. 12A), with its northern extent located beyond the limit of the 3D seismic survey (Fig. 12A). F7 is physically connected to the underlying Type 1 structure for its entire length and strikes approximately parallel to it (i.e. N165°; Fig. 12E). Similar to faults physically connected to the Type 2 structures (i.e. F3-6), F7 is characterised by negative throw values (up to -60 m) and expansion index values <1 immediately above Top Basement (Figs. 12C and D). Approximately 1300 m above Top Basement, F7 splays upwards into three, left-stepping, en-echelon segments (F7a-c; Fig. 12A), which extend to the Intra-Giant Foresets Formation horizon (Fig. 12F). However, at this structural level, segments F7a-c strike N180°, oblique to and defining a 15° clockwise rotation from the lowermost part of the fault (cf. Figs. 12E and F), resulting in twisting of the fault surface. Furthermore, the upper segments dip more gently than the lower part of the fault, resulting in a broadly sigmoidal cross-sectional geometry (Fig. 12B). The T-z plot reveals a B-shaped throw profile, with two throw maxima (*c.* 60-80 m) in Eocene and Miocene strata (Fig. 12C). On the fault surface, the lower throw maximum extends laterally for almost the entire fault length, whereas we observe three discrete throw maxima in the Miocene succession, corresponding to the individual segments (F7a-c; Fig. 12A).

8. Interpretation and Discussion

8.1. Growth History of Normal Faults

The cover normal faults physically disconnected from the intra-basement structures (e.g. F1 and F2; Fig. 9) show a more regular throw distribution than those are physically connected (e.g. F3-7; Figs. 10, 11, 12). The former display a single throw maximum in the Miocene sedimentary sequence that decreases radially towards the tip line (Fig. 9), whereas the latter display an area of negative throw at the base of the fault plane (i.e. in Paleocene strata, 200-300 m above Top Basement; Figs. 10, 11 and 12), with a positive throw maximum located in Eocene strata (400-500 m above Top Basement; Figs. 10, 11 and 12). Of the faults physically connected to intra-basement structures, some display a single throw maximum in Eocene sedimentary sequence (Fig. 10), whereas others display an additional throw maximum in Miocene sedimentary cover, resulting in B-shaped throw profiles (Figs. 11 and 12). Importantly, the areas of negative throw at the fault base are commonly overlain by folds (Figs. 4C and D), suggesting: (i) intra-basement structures were compressionally reactivated during late Miocene inversion and propagated upwards into the sedimentary cover as blind structures, resulting in fault-propagation folds (e.g. Mitra, 1990; Erslev and Mayborn, 1997; Figs. 13 A and B); and (ii) intra-basement structures were slightly, if at all, extensionally reactivated during Plio-Pleistocene rifting, as any hypothetical normal slip must be smaller than the late Miocene reverse displacement (Fig. 13C). We consider this lack of or only very limited extensional reactivation reflects: (i) the shallow dip of intra-basement structures (20°-30°, Fig. 4), making them unfavourable structures to accommodate extension (Sibson, 1985); and (ii) the relatively small amount of regional extension (low beta-factor) accommodated in the Taranaki Basin during the Plio-Pleistocene (Giba *et al.*, 2010).

Given the lack of evidence for significant extensional reactivation of the intra-basement structures, we infer the cover normal faults preserved broadly the original throw distribution, which can thus be used to infer their growth history (cf. Deng *et al.*, 2017). Hence, we interpret that the lower (i.e. Eocene) and the upper (i.e. Miocene) throw maxima represent nucleation of normal faults in Eocene and Miocene sedimentary succession, respectively (cf. Mansfield and Cartwright, 1996; Hongxing and Anderson, 2007). Normal faults must necessarily initiate after the deposition of the stratigraphic package hosting their nucleation sites; this implies that normal faults with nucleation sites in Miocene strata formed during the Plio-Pleistocene rifting event, whereas normal faults with nucleation sites in Eocene strata reflect Cretaceous-Early Eocene or the Plio-Pleistocene extension. However, rift-related extensional activity ceased by the end of the Paleocene in the western part of the Taranaki

Basin (Strogen *et al.*, 2017), where our study area is located (Fig. 1). Furthermore, in the Paleocene interval we see no fault-related thickness variations that could be attributed to normal faulting of this age (Fig. 8A). These stratigraphic considerations suggest the studied normal fault network formed during the Plio-Pleistocene rifting event (Fig. 13C). Furthermore, Plio-Pleistocene normal faulting is clearly indicated by distinct fault-related thickness variations (Fig. 8) and, in some cases, by flat upper tiplines associated with steep throw gradient (Fig. 9; cf. Nicol *et al.*, 1996; Childs *et al.*, 2003; Baudon and Cartwright, 2008c). However, we cannot rule out that some normal faults first developed during Paleocene-Early Eocene rifting and were subsequently compressionaly reactivated during late Miocene inversion. The B-shaped profiles of some normal faults physically connected to intra-basement structures (Figs. 11 and 12) likely reflect dip linkage between initially isolated, and occasionally still partly disconnected (Fig. 11), fault segments that nucleated in Eocene and Miocene sedimentary succession. Importantly, our stratigraphic considerations suggest the lower and the upper fault segments developed during the same rifting event (i.e. Plio-Pleistocene rifting), implying they may have been kinematic coupled (Fig. 13, case 2). However, the normal faults disconnected from intra-basement structures, which nucleated in the upper part of the cover (i.e. in the Miocene sedimentary succession), grew freely by simple radial tip line propagation, suggesting only limited mechanical and kinematic constraints by deeper fault segments as well as intra-basement structures (Fig. 13C, case 1).

8.2. Influence of Intra-basement Structures on Normal Faulting

Having established that the studied normal fault network largely developed during a single phase of Plio-Pleistocene extension, we argue that the variability of fault strikes within this relatively small area (Fig. 7) reflects the variable influence of pre-existing mechanical anisotropies in the underlying basement rocks, rather than a temporal or spatial change of extension direction. Given the intra-basement structures have been poorly, if at all, extensionally reactivated during the Plio-Pleistocene rifting event, their influence on the development of normal faults cannot be explained by simple extensional reactivation and upward propagation. Hence, other processes must be invoked to explain the spatial correlation and the physical connectivity between intra-basement structures and cover faults (Figs. 10, 11 and 12). The negative throw region just above the physical connection to intra-basement structures (Figs. 10, 11 and 12) suggests that cover faults initiated as thrusts due to late Miocene reverse reactivation and upward propagation of intra-basement structures. The sharp transition from this negative throw region to elongated positive throw maxima (Figs. 10, 11 and 12) indicates that Plio-Pleistocene normal faults nucleated at a short distance away, and possibly directly, from the upper tip of late Miocene thrusts. The localisation of new normal faults at a short distance from pre-existing structures may reflect: (i) accumulation of stress on pre-existing structures (i.e. intra-basement structures and the overlying late Miocene thrusts; Jackson and Rotevatn, 2013); (ii) and, possibly, preferential nucleation of new normal faults from pre-existing weak anisotropies (i.e. late Miocene thrusts).

A variety of mechanisms can contribute to the nucleation of faults within the damage zones of thrusts and folds, rather than within intact country rock: (i) strength reduction due to pervasive fracturing (e.g. Gudmundsson, 2011; Sun *et al.*, 2017); (ii) reduction of the effective stress due to higher permeability and pore fluid pressure (e.g. Sibson, 1995); and (iii) a range of strain weakening effects, including gouge formation, mineral transformation and microstructural re-arrangement (e.g. Bos and Spiers, 2002). The positive feedback between these processes may result in propagation and linkage of fractures, leading to the final development of through-going faults (cf. Vass *et al.*, 2014). The nucleation of normal faults at the upper tips of deeper lying, pre-existing thrusts is also observed in both physical models of and natural examples presented by Faccenna *et al.* (1995). Furthermore, these models support the possibility that new normal faults can nucleate also from pre-existing structures that do not undergo extensional reactivation. In a more general sense, nucleation of new normal faults from pre-existing structures has been widely documented during multiphase extension, with new normal faults nucleating from older normal faults (e.g. Henza *et al.*, 2010; Duffy *et al.*, 2015; Withjack *et al.*, 2017). Interestingly, when normal faults emanated from pre-existing structures striking nearly perpendicularly to the Plio-Pleistocene extension direction (i.e. NW-SE; Giba *et al.*, 2012), they propagated to the upper part of the cover through nucleation and dip linkage of kinematically related segments (Fig. 11). In contrast, when normal faults emanated from pre-existing structures striking strongly obliquely to the Plio-Pleistocene extension direction, they remained restricted to the lower part of the cover (Fig. 10). This selective upward propagation of normal faults suggests the regional stress field becomes dominant over the intra-basement structures as distance from the latter increases, allowing only for favourably oriented structures to propagate to the upper part of the cover (Fig. 13C, case 2). The dominant influence of the regional stress field in the upper part of the cover is supported also by the nucleation and growth of optimally-oriented (i.e. NE/NNE-striking) normal faults in the Miocene-Pliocene sedimentary succession (Fig. 13C, case 1).

8.3. Evidence for km-scale perturbation of the regional stress field

We have now established the general geometric and kinematic relationships between intra-basement structures and cover normal faults. However, the 3D geometry and throw distribution on the cover faults physically connected to the Type 1 intra-basement structure (i.e. the 2.5 km wide package of reflections in the northern part of the study area) suggest a more complex relationship, with additional mechanisms acting in this case. The faults physically connected to the Type 1 structure (i.e. F7, F7a-c; Fig. 12) are the only normal faults oblique to the Plio-Pleistocene extension direction (i.e. NW-SE; Giba *et al.*, 2012) that propagated through the entire sedimentary succession (Fig. 13C, case 3). Furthermore, differently from the other cover faults they display a clear up-sequence rotation of fault strike, with the obliquity to the Plio-Pleistocene extension direction decreasing progressively towards the upper part of the sedimentary cover (cf. Figs. 12E and F). Similar up-sequence strike rotation has been interpreted to reflect emanation and upward propagation of new normal faults from pre-existing, buried, oblique structures (Giba *et al.*, 2012; Withjack *et al.*, 2017). However, our kinematic analysis indicates that F7, F7a-c likely initiated as isolated segments that eventually linked to form a single, somewhat sigmoidal fault plane. Hence, new normal faults geometrically and kinematically related to the intra-basement structures (i.e. F7a-c) appear to have nucleated at a significant distance from the latter (c. 1500 m), propagating to the upper part of the cover (Fig. 12). Such far-reaching influence of the intra-basement structures on normal fault geometry suggests local perturbation of the overall rift-related stress field extended a considerable distance up into the sedimentary cover. In contrast the oblique normal faults physically connected to Type 2 intra-basement structures have limited vertical extent (<1500 m above Top Basement; Fig. 10); this implies any hypothetical local perturbation of the stress field associated with the Type 2 structures must have been restricted to only a few hundreds metres above Top Basement. Our work suggests that the width of intra-basement structures exerts a first-order control on the magnitude of the stress field perturbation, with only km-wide intra-basement structures capable of determining stress-field perturbation affecting substantial thicknesses of the cover succession. Stress field perturbations originated by similar km-wide intra-basement structures are also suggested by Phillips *et al.* (2016) based on the geometric relationship with the overlying normal faults. Furthermore, Morley (2004) suggests that km-wide perturbation of the stress field can be related to pervasive intra-basement fabrics, which are reasonably expected within a stack of mylonites inferred to define the Type 1 structure.

8.4. Implications for non-colinear rift fault network

We reconstructed the evolution of a non-colinear rift fault network overlying crystalline basement, highlighting different geometric and kinematic relationships between normal faults and intra-basement structures (Fig. 13). Non-colinear rift fault networks can develop both in single-phase and multiphase rifts (Reeve *et al.*, 2015). In single-phase rifts, non-colinear fault systems are generally only locally developed, typically associated with stress pertubations adjacent to major faults (Duffy *et al.*, 2015). However, our study suggests that the influence of intra-basement structures can lead to the development of pervasive non-colinear fault networks (Fig. 7B) during a single rifting event. In similar cases, discriminating between single-phase and multiphase fault networks is not straightforward, and discerning the influence of intra-basement structures on normal faults development is thus crucial.

The best way to determine whether underlying intra-basement structures influence the development of the overlying rift-related normal fault network is by comparing the distribution and geometry or both sets of structures, and, if possible, their kinematics. However, intra-basement structures are often poorly imaged in seismic data and are rarely preserved along with the overlying normal faults in the same outcrop, implying we typically rely on only qualitative correlation between seismically imaged normal faults and basement tectonic trends observed onshore (e.g. Roberts and Holdsworth, 1999; Wilson *et al.*, 2006). By comparing the basement-influenced fault network in our study area with the multiphase fault network described by Duffy *et al.* (2015), we propose some key-characteristics that could help determine the origin of a non-colinear fault network, when knowledge of the intra-basement structures is not accessible. For example, in multiphase rifts, the most common linkage style is represented by sharp, abutting intersections, with the second stage faults having a single throw maximum near the branchline (Duffy *et al.*, 2015). In contrast, in our study, no abutting intersections are observed, fault strike changes gradually along the fault length (Fig. 7B), and throw maxima are positioned near the fault centres (Figs. 9, 10, 11 and 12). In addition to the interaction styles and the kinematics, the vertical extent of the non-colinear fault network may also help to discriminate between different causal mechanisms. In fact, the influence of intra-basement structures appears to have a limited vertical extent, resulting in non-colinear fault network restricted to the lower part of the sedimentary cover.

9. Conclusions

Based on the integration of time-structure maps, cross-sections and detailed 3D kinematic analyses, we draw the following key conclusions regarding the influence of intra-basement structures on the development of rift-related normal faults in the Taranaki Basin, offshore New Zealand:

1. In the study area, intra-basement structures appear to have played a key role during the Plio-Pleistocene rifting, as suggested by several normal faults mimicking the underlying intra-basement structures and physically connected to them. This resulted in non-collinear faulting, with normal faults striking obliquely to the regional trend of the rift. However, in the upper part of the cover there are also normal faults that do not seem to be affected by intra-basement structures.
2. The normal faults physically connected to underlying intra-basement structures typically show a sharp transition from positive to negative throw near Top Basement. Negative throw is interpreted as the result of compressive reactivation and upward

propagation of the intra-basement structures during the late Miocene. The preservation of the original negative throw suggests that intra-basement structures were not significantly reactivated during the Plio-Pleistocene rifting. This implies that extensional reactivation is not a fundamental condition for intra-basement structures to have an influence on rift-related normal faults.

3. The normal faults physically connected to intra-basement structures display throw maxima (i.e. nucleation points) at a short distance (100-200 m) from, and with approximately the same lateral extent as, the area of negative throw just above Top Basement. This throw distribution suggests that during the Plio-Pleistocene rifting normal faults nucleated from underlying late Miocene reverse structures, which resulted from preceding reactivation and upward propagation of intra-basement structures.
4. Our kinematic analysis highlighted the development of normal faults striking parallel to the underlying Type 1 intra-basement structure and obliquely to the regional trend of the rift, although the nucleation points are located 1500 m above Top Basement. This far-reaching influence over normal faults suggests that the Type 1 structure perturbed the local stress field throughout the whole sedimentary cover. No similar effect has been observed in association with Type 2 structures, suggesting that only km-wide intra-basement structures, like Type 1, can originate long-length perturbation of the stress field.
5. Nucleation from pre-existing structures and perturbation of the local stress field can be the core of the influence of basement structures on rift-related faults and not just ancillary processes with respect to simple reactivation. Future models for structural inheritance in rifting settings should incorporate long-length influence of pre-existing structures and kinematic coupling between structures at different levels. Kinematic

analysis proved to be a fundamental tool to extract information from 3D seismic data, posing important constraints to analogue and numerical models.

Acknowledgements

Funding for this research was primarily provided by the University of Padova and the Aldo Gini Foundation in the form of a studentship awarded to Luca Collanega. We would like to thank Matteo Massironi, Thomas Phillips, Dancho Azagra and Josè Reis for insightful discussions during the course of this work. We also thank Schlumberger (Petrel) and Badley Geoscience (T7) for providing access to software.

References

ARBARET, L. & BURG, J.P. (2003) Complex Flow in Lowest Crustal, Anastomosing Mylonites: Strain Gradients in a Kohistan Gabbro, Northern Pakistan: Lower Crustal Shear Zones in the Kohistan Island Arc. *Journal of Geophysical Research: Solid Earth*, **108**.

BARTHOLOMEW, I.D., PETERS, J.M. & POWELL, C.M. (1993) Regional structural evolution of the North Sea: oblique slip and reactivation of basement lineaments. In: *Petroleum Geology of Northwest Europe, Proceedings of the 4th Conference* (Ed. by J.R. Parker) Geological Society, London, Special Publications, 1109-1122.

BAUDON, C. & CARTWRIGHT, J. (2008) The Kinematics of Reactivation of Normal Faults Using High Resolution Throw Mapping. *Journal of Structural Geology*, **30,** 1072-1084.

BAUDON, C. & CARTWRIGHT, J. (2008) Early Stage Evolution of Growth Faults: 3D Seismic Insights from the Levant Basin, Eastern Mediterranean. *Journal of Structural Geology*, **30,** 888-898.

BAUDON, C. & CARTWRIGHT, J.A. (2008) 3D Seismic Characterisation of an Array of Blind

Normal Faults in the Levant Basin, Eastern Mediterranean. *Journal of Structural Geology*, **30,** 746-760.

BIRD, P.C., CARTWRIGHT, J.A. & DAVIES, T.L. (2015) Basement Reactivation in the Development of Rift Basins: An Example of Reactivated Caledonide Structures in the West Orkney Basin. *Journal of the Geological Society*, **172,** 77-85.

BRADSHAW, J.D., PANKHURST, R.J., WEAVER, S.D., STOREY, B.C., MUIR, R.J., IRELAND, T.R. (1997) New Zealand Superterranes Recognized in Marie Byrd Land and Thurston Island. *Terra Antartica*, **3,** 429-436.

BRADSHAW, J.D. (1989) Cretaceous Geotectonic Patterns in the New Zealand Region. *Tectonics*, **8,** 803-820.

BRADSHAW, J.D. (1993) A Review of the Median Tectonic Zone: Terrane Boundaries and Terrane Amalgamation near the Median Tectonic Line. *New Zealand Journal of Geology and Geophysics*, **36,** 117-125.

BRANDES, C. & TANNER, D.C. (2014) Fault-Related Folding: A Review of Kinematic Models and Their Application. *Earth-Science Reviews*, **138,** 352-370.

BREWER, J.A., MATTHEWS, D.H., WARNER, M.R., HALL, J., SMYTHE, D.K. & WHITTINGTON, R.J. (1983) Birps Deep Seismic Reflection Studies of the British Caledonides. *Nature*, **305,** 206-210.

BROCHER, T.M. & CHRISTENSEN, N.I. (1990) Seismic Anisotropy Due to Preferred Mineral Orientation Observed in Shallow Crustal Rocks in Southern Alaska. *Geology*, **18,** 737.

CARRERAS, J., CZECK, D.M., DRUGUET, E. & HUDLESTON, P.J. (2010) Structure and Development of an Anastomosing Network of Ductile Shear Zones. *Journal of Structural Geology*, **32,** 656-666.

CARTWRIGHT, J.A., TRUDGILL, B.D. & MANSFIELD, C.S. (1995) Fault Growth by Segment Linkage: An Explanation for Scatter in Maximum Displacement and Trace Length Data from the Canyonlands Grabens of Se Utah. *Journal of Structural Geology*, **17,** 1319-1326.

CHENRAI, P. & HUUSE, M. (2017) Pockmark Formation by Porewater Expulsion during Rapid Progradation in the Offshore Taranaki Basin, New Zealand. *Marine and Petroleum Geology*, **82,** 399-413.

CHILDS, C., NICOL, A., WALSH, J.J. & WATTERSON, J. (2003) The Growth and Propagation of Synsedimentary Faults. *Journal of Structural Geology*, **25,** 633-648.

CLARINGBOULD, J.S., BELL, R.E., JACKSON, C.A.-L., GAWTHORPE, R.L. & ODINSEN, T. (2017) Pre-Existing Normal Faults Have Limited Control on the Rift Geometry of the Northern North Sea. *Earth and Planetary Science Letters*, **475,** 190-206.

CONNEALLY, J., CHILDS, C. & WALSH, J.J. (2014) Contrasting Origins of Breached Relay Zone Geometries. *Journal of Structural Geology*, **58,** 59-68.

DENG, C., GAWTHORPE, R.L., FINCH, E. & FOSSEN, H. (2017) Influence of a Pre-Existing Basement Weakness on Normal Fault Growth during Oblique Extension: Insights from Discrete Element Modeling. *Journal of Structural Geology*, **105,** 44-61.

DESTRO, N. (1995) Release Fault: A Variety of Cross Fault in Linked Extensional Fault Systems, in the Sergipe-Alagoas Basin, Ne Brazil. *Journal of Structural Geology*, **17,** 615-629.

DUFFY, O.B., BELL, R.E., JACKSON, C.A.-L., GAWTHORPE, R.L. & WHIPP, P.S. (2015) Fault Growth and Interactions in a Multiphase Rift Fault Network: Horda Platform, Norwegian North Sea. *Journal of Structural Geology*, **80,** 99-119.

ERSLEV, E.A. & MAYBORN, K.R. (1997) Multiple Geometries and Modes of Fault-Propagation Folding in the Canadian Thrust Belt. *Journal of Structural Geology*, **19,** 321-335.

FACCENNA, C., NALPAS, T., BRUN, J.-P., DAVY, P. & BOSI, V. (1995) The Influence of Pre-Existing Thrust Faults on Normal Fault Geometry in Nature and in Experiments.

Journal of Structural Geology, **17,** 1139-1149.

FAZLIKHANI, H., FOSSEN, H., GAWTHORPE, R.L., FALEIDE, J.I. & BELL, R.E. (2017) Basement Structure and Its Influence on the Structural Configuration of the Northern North Sea Rift. *Tectonics*, **36,** 2017TC004514.

FOSSEN, H., KHANI, H.F., FALEIDE, J.I., KSIENZYK, A.K. & DUNLAP, W.J. (2017) Post-Caledonian Extension in the West Norway–Northern North Sea Region: The Role of Structural Inheritance. *Geological Society, London, Special Publications*, **439,** 465-486.

FOUNTAIN, D.M., HURICH, C.A. & SMITHSON, S.B. (1984) Seismic Reflectivity of Mylonite Zones in the Crust. *Geology*, **12,** 195.

GERNIGON, L., BRÖNNER, M., ROBERTS, D., OLESEN, O., NASUTI, A. & YAMASAKI, T. (2014) Crustal and Basin Evolution of the Southwestern Barents Sea: From Caledonian Orogeny to Continental Breakup. *Tectonics*, **33,** 2013TC003439.

GIBA, M., NICOL, A. & WALSH, J.J. (2010) Evolution of Faulting and Volcanism in a Back-Arc Basin and Its Implications for Subduction Processes. *Tectonics*, **29,** TC4020.

GIBA, M., WALSH, J.J. & NICOL, A. (2012) Segmentation and Growth of an Obliquely Reactivated Normal Fault. *Journal of Structural Geology*, **39,** 253-267.

GUPTA, A. & SCHOLZ, C.H. (2000) A Model of Normal Fault Interaction Based on Observations and Theory. *Journal of Structural Geology*, **22,** 865-879.

GUDMUNDSSON, A. (2011) *Rock fractures in Geological Processes*. Cambridge University Press, Cambridge.

HANSEN, R.J. & KAMP, P.J. (2002) Evolution of the Giant Foresets Formation, Northern Taranaki Basin, New Zealand.

HANSEN, R.J. & KAMP, P.J. (2004) Rapid Progradation of the Pliocene-Pleistocene Continental Margin, Northern Taranaki Basin, New Zealand, and Implications. *Proceedings of New Zealand Petroleum Conference*, 1-9.

HENZA, A.A., WITHJACK, M.O. & SCHLISCHE, R.W. (2010) Normal-Fault Development during Two Phases of Non-Coaxial Extension: An Experimental Study. *Journal of Structural Geology*, **32,** 1656-1667.

HENZA, A.A., WITHJACK, M.O. & SCHLISCHE, R.W. (2011) How Do the Properties of a Pre-Existing Normal-Fault Population Influence Fault Development During a Subsequent Phase of Extension? *Journal of Structural Geology*, **33,** 1312-1324.

HOMBERG, C., HU, J.C., ANGELIER, J., BERGERAT, F. & LACOMBE, O. (1997) Characterization of Stress Perturbations near Major Fault Zones: Insights from 2-D Distinct-Element Numerical Modelling and Field Studies (Jura Mountains). *Journal of Structural Geology*, **19,** 703-718.

HONGXING, G. & ANDERSON, J.K. (2007) Fault Throw Profile and Kinematics of Normal Fault: Conceptual Models and Geologic Examples. *Geol. J. China Univ.*, **13,** 75-88.

HURICH, C.A., SMITHSON, S.B., FOUNTAIN, D.M. & HUMPHREYS, M.C. (1985) Seismic Evidence of Mylonite Reflectivity and Deep Structure in the Kettle Dome Metamorphic Core Complex, Washington. *Geology*, **13,** 577.

JACKSON, C.A.-L. & ROTEVATN, A. (2013) 3D Seismic Analysis of the Structure and Evolution of a Salt-Influenced Normal Fault Zone: A Test of Competing Fault Growth Models. *Journal of Structural Geology*, **54,** 215-234.

KIMBROUGH, D.L., TULLOCH, A.J., GEARY, E., COOMBS, D.S. & LANDIS, C.A. (1993) Isotopic Ages from the Nelson Region of South Island New Zealand: Crustal Structure and Definition of the Median Tectonic Zone. *Tectonophysics*, **225,** 433-448.

KING, P.R., THRASHER, G.P. (1996) *Cretaceous-Cenozoic geology and petroleum systems of the Taranaki Basin, New Zealand*. Institute of Geological and Nuclear Sciences Monographs, 13.

KING, R.C., TINGAY, M.R.P., HILLIS, R.R., MORLEY, C.K. & CLARK, J. (2010) Present-Day Stress

Orientations and Tectonic Provinces of the NW Borneo Collisional Margin. *Journal of Geophysical Research: Solid Earth*, **115,** B10415.

KIRKPATRICK, J.D., BEZERRA, F.H.R., SHIPTON, Z.K., DO NASCIMENTO, A.F., PYTHAROULI, S.I., LUNN, R.J. & SODEN, A.M. (2013) Scale-Dependent Influence of Pre-Existing Basement Shear Zones on Rift Faulting: A Case Study from Ne Brazil. *Journal of the Geological Society*, **170,** 237-247.

KLEMPERER, S.L. & GROUP1, B. (1987) Reflectivity of the Crystalline Crust: Hypotheses and Tests. *Geophysical Journal International*, **89,** 217-222.

KORME, T., ACOCELLA, V. & ABEBE, B. (2004) The Role of Pre-Existing Structures in the Origin, Propagation and Architecture of Faults in the Main Ethiopian Rift. *Gondwana Research*, **7,** 467-479.

MAERTEN, L., WILLEMSE, E.J.M., POLLARD, D.D. & RAWNSLEY, K. (1999) Slip Distributions on Intersecting Normal Faults. *Journal of Structural Geology*, **21,** 259-272.

MAERTEN, L., GILLESPIE, P. & POLLARD, D.D. (2002) Effects of Local Stress Perturbation on Secondary Fault Development. *Journal of Structural Geology*, **24,** 145-153.

MANSFIELD, C.S. & CARTWRIGHT, J.A. (1996) High Resolution Fault Displacement Mapping from Three-Dimensional Seismic Data: Evidence for Dip Linkage during Fault Growth. *Journal of Structural Geology*, **18,** 249-263.

MCDONOUGH, D.T. & FOUNTAIN, D.M. (1988) Reflection Characteristics of a Mylonite Zone Based on Compressional Wave Velocities of Rock Samples. *Geophysical Journal International*, **93,** 547-558.

MITRA, S. (1990) Fault-propagation folds: geometry, kinematic evolution, and hydrocarbon traps. *AAPG Bull.*, **74,** 921-945.

MODISI, M.P., ATEKWANA, E.A., KAMPUNZU, A.B. & NGWISANYI, T.H. (2000) Rift Kinematics during the Incipient Stages of Continental Extension: Evidence from the Nascent

Okavango Rift Basin, Northwest Botswana. *Geology*, **28,** 939.

MOORE, M.E., GLEADOW, A.J.W. & LOVERING, J.F. (1986) Thermal Evolution of Rifted Continental Margins: New Evidence from Fission Tracks in Basement Apatites from Southeastern Australia. *Earth and Planetary Science Letters*, **78,** 255-270.

MORLEY, C.K., HARANYA, C., PHOOSONGSEE, W., PONGWAPEE, S., KORNSAWAN, A. & WONGANAN, N. (2004) Activation of Rift Oblique and Rift Parallel Pre-Existing Fabrics During Extension and Their Effect on Deformation Style: Examples from the Rifts of Thailand. *Journal of Structural Geology*, **26,** 1803-1829.

MORLEY, C.K. (2010) Stress Re-Orientation along Zones of Weak Fabrics in Rifts: An Explanation for Pure Extension in 'Oblique' Rift Segments? *Earth and Planetary Science Letters*, **297,** 667-673.

MORTIMER, N., TULLOCH, A.J. & IRELAND, T.R. (1997) Basement Geology of Taranaki and Wanganui Basins, New Zealand. *New Zealand Journal of Geology and Geophysics*, **40,** 223-236.

MORTIMER, N., TULLOCH, A.J., SPARK, R.N., WALKER, N.W., LADLEY, E., ALLIBONE, A. & KIMBROUGH, D.L. (1999) Overview of the Median Batholith, New Zealand: A New Interpretation of the Geology of the Median Tectonic Zone and Adjacent Rocks. *Journal of African Earth Sciences*, **29,** 257-268.

MOUSLOPOULOU, V., NICOL, A., WALSH, J.J., BEGG, J.G., TOWNSEND, D.B. & HRISTOPULOS, D.T. (2012) Fault-Slip Accumulation in an Active Rift over Thousands to Millions of Years and the Importance of Paleoearthquake Sampling. *Journal of Structural Geology*, **36,** 71-80.

MUIR, R.J., BRADSHAW, J.D., WEAVER, S.D. & LAIRD, M.G. (2000) The Influence of Basement Structure on the Evolution of the Taranaki Basin, New Zealand. *Journal of the Geological Society*, **157,** 1179-1185.

MURAOKA, H. & KAMATA, H. (1983) Displacement Distribution Along Minor Fault Traces. *Journal of Structural Geology*, **5,** 483-495.

NICOL, A., WATTERSON, J., WALSH, J.J. & CHILDS, C. (1996) The Shapes, Major Axis Orientations and Displacement Patterns of Fault Surfaces. *Journal of Structural Geology*, **18,** 235-248.

NICOL, A., WALSH, J., BERRYMAN, K. & NODDER, S. (2005) Growth of a Normal Fault by the Accumulation of Slip over Millions of Years. *Journal of Structural Geology*, **27,** 327-342.

PEACE, A., MCCAFFREY, K., IMBER, J., VAN HUNEN, J., HOBBS, R. & WILSON, R. (2017) The Role of Pre-Existing Structures During Rifting, Continental Breakup and Transform System Development, Offshore West Greenland. *Basin Research*.

PHILLIPS, T.B., JACKSON, C.A.-L., BELL, R.E., DUFFY, O.B. & FOSSEN, H. (2016) Reactivation of Intrabasement Structures During Rifting: A Case Study from Offshore Southern Norway. *Journal of Structural Geology*, **91,** 54-73.

PHILLIPS, T.B., JACKSON, C.A.-L., BELL, R.E. & DUFFY, O.B. (2018) Oblique Reactivation of Lithosphere-Scale Lineaments Controls Rift Physiography – the Upper-Crustal Expression of the Sorgenfrei–Tornquist Zone, Offshore Southern Norway. *Solid Earth*, **9,** 403-429.

RAIT, G., CHANIER, F. & WATERS, D.W. (1991) Landward- and Seaward-Directed Thrusting Accompanying the Onset of Subduction beneath New Zealand. *Geology*, **19,** 230.

REEVE, M.T., BELL, R.E., DUFFY, O.B., JACKSON, C.A.-L. & SANSOM, E. (2015) The Growth of Non-Colinear Normal Fault Systems; What Can We Learn from 3D Seismic Reflection Data? *Journal of Structural Geology*, **70,** 141-155.

REILLY, C., NICOL, A., WALSH, J.J. & SEEBECK, H. (2015) Evolution of Faulting and Plate Boundary Deformation in the Southern Taranaki Basin, New Zealand. *Tectonophysics*, **651-652,** 1-18.

RENNIE, S.F., FAGERENG, Å. & DIENER, J.F.A. (2013) Strain Distribution within a Km-Scale, Mid-Crustal Shear Zone: The Kuckaus Mylonite Zone, Namibia. *Journal of Structural Geology*, **56,** 57-69.

RING, U. (1994) The Influence of Preexisting Structure on the Evolution of the Cenozoic Malawi Rift (East African Rift System). *Tectonics*, **13,** 313-326.

ROBERTS, A.M. & HOLDSWORTH, R.E. (1999) Linking Onshore and Offshore Structures: Mesozoic Extension in the Scottish Highlands. *Journal of the Geological Society*, **156,** 1061-1064.

ROBIN, P.-Y.F. (1979) Theory of Metamorphic Segregation and Related Processes. *Geochimica et Cosmochimica Acta*, **43,** 1587-1600.

SIBSON, R.H. (1985) A Note on Fault Reactivation. *Journal of Structural Geology*, **7,** 751-754.

SIBSON, R.H. (1995) Selective Fault Reactivation during Basin Inversion: Potential for Fluid Redistribution through Fault-Valve Action. *Geological Society, London, Special Publications*, **88,** 3-19.

SIUDA, K., MAGEE, C., BELL, R., JACKSON, C.A-L. & COLLANEGA, L. (in review). Pre-existing basement thrusts influence rifting in the Taranaki Basin, New Zealand. Preprint available on EarthArXiv (http://doi.org/10.17605/OSF.IO/5E9Q6)

STAGPOOLE, V. & NICOL, A. (2008) Regional Structure and Kinematic History of a Large Subduction Back Thrust: Taranaki Fault, New Zealand. *Journal of Geophysical Research*, **113**.

STROGEN, D.P. (2011) *Updated Paleogeographic Maps for the Taranaki Basin and Surrounds*. Lower Hutt, New Zealand: GNS Science.

STROGEN, D.P., BLAND, K.J., NICOL, A. & KING, P.R. (2014) Paleogeography of the Taranaki Basin Region during the Latest Eocene–Early Miocene and Implications for the 'Total Drowning' of Zealandia. *New Zealand Journal of Geology and Geophysics*, **57,** 110-127.

STROGEN, D.P., SEEBECK, H., NICOL, A. & KING, P.R. (2017) Two-Phase Cretaceous–Paleocene Rifting in the Taranaki Basin Region, New Zealand; Implications for Gondwana Break-Up. *Journal of the Geological Society*, **174,** 929-946.

SUN, S., HOU, G. & ZHENG, C. (2017) Fracture Zones Constrained by Neutral Surfaces in a Fault-Related Fold: Insights from the Kelasu Tectonic Zone, Kuqa Depression. *Journal of Structural Geology*, **104,** 112-124.

TAYLOR, S.K., NICOL, A. & WALSH, J.J. (2008) Displacement Loss on Growth Faults Due to Sediment Compaction. *Journal of Structural Geology*, **30,** 394-405.

TRUDGILL, B.D. (2002) Structural Controls on Drainage Development in the Canyonlands Grabens of Southeast Utah. *AAPG Bulletin*, **86,** 1095-1112.

VASS, A., KOEHN, D., TOUSSAINT, R., GHANI, I. & PIAZOLO, S. (2014) The Importance of Fracture-Healing on the Deformation of Fluid-Filled Layered Systems. *Journal of Structural Geology*, **67,** 94-106.

WALSH, J.J. & WATTERSON, J. (1987) Distributions of Cumulative Displacement and Seismic Slip on a Single Normal Fault Surface. *Journal of Structural Geology*, **9,** 1039-1046.

WALSH, J.J. & WATTERSON, J. (1991) Geometric and Kinematic Coherence and Scale Effects in Normal Fault Systems. *Geological Society, London, Special Publications*, **56,** 193-203.

WALSH, J.J., BAILEY, W.R., CHILDS, C., NICOL, A. & BONSON, C.G. (2003) Formation of Segmented Normal Faults: A 3-D Perspective. *Journal of Structural Geology*, **25,** 1251-1262.

WANG, C.-Y., OKAYA, D.A., RUPPERT, C., DAVIS, G.A., GUO, T.-S., ZHONG, Z. & WENK, H.-R. (1989) Seismic Reflectivity of the Whipple Mountain Shear Zone in Southern California. *Journal of Geophysical Research: Solid Earth*, **94,** 2989-3005.

WILSON, R.W., MCCAFFREY, K.J.W., HOLDSWORTH, R.E., IMBER, J., JONES, R.R., WELBON, A.I.F. & ROBERTS, D. (2006) Complex Fault Patterns, Transtension and Structural

Segmentation of the Lofoten Ridge, Norwegian Margin: Using Digital Mapping to Link Onshore and Offshore Geology: Transtension and Segmentation in Lofoten. *Tectonics*, **25,** n/a-n/a.

WITHJACK, M.O., HENZA, A.A. & SCHLISCHE, R.W. (2017) Three-Dimensional Fault Geometries and Interactions within Experimental Models of Multiphase Extension. *AAPG Bulletin*, **101,** 1767-1789.

Caption Section

Fig. 1. Map illustrating the main structural elements of the Southern Taranaki Basin (modified from Miur *et al.,* 2000). Underlying basement terranes are shown in grey. Note the plan-view correlation between basin-bounding faults and basement terrane boundaries. The red box indicates the location of the 3D seismic survey. Inset – plate tectonic setting of the Taranaki Basin. Note the location of the Taranaki Basin between the Tasman Sea Rift and the Pacific Plate Subduction Zone.

Fig. 2. Stratigraphic and structural setting of the study area. (A) Stratigraphic framework indicating the interpreted seismic reflection events. The Maui-6 synthetic seismogram, which was used to tie the seismic reflection data to stratigraphic data, is also shown. Seismic-stratigraphic packages are correlated to the major regional tectonic events, using biostratigraphic data provided in well Maui-3 (location of wells shown in Fig. 3). The stratigraphic position of key TWT-structure maps (i.e. Figs. 5, 6 and 7) and time-thickness maps (i.e. Fig. 8) presented in this study are also shown. (B) Regional seismic line showing the structural setting of the study area and the main stratigraphic units (location shown in Fig. 1; see Appendix A for enlarged uninterpreted and interpreted versions of this section). Note the position of the study area in the uplifted footwall of the Cape Egmont Fault and the low-strain,

stratigraphically simple setting (stratigraphic correlation across the Cape Egmont Fault based on Nicol *et al.*, 2005).

Fig. 3. Map illustrating the location of the 3D seismic survey and wells used in this study.

Fig. 4. Series of uninterpreted seismic profiles and geo-seismic sections illustrating the key characteristics of intra-basement reflections (locations of sections shown in Fig. 5C; see Appendix A for enlarged uninterpreted and interpreted versions of the sections). (A) Seismic and geo-seismic section oriented orthogonal to the Type 1 reflections in the northern part of the survey area. Note the linkage between the Type 1 reflections and the overlying normal fault. (B) Seismic and geo-seismic section oriented orthogonal to Type 2 and Type 3 reflections in the centre of the survey area. (C) Close-up of the Type 1 reflections. Note the high-amplitude reflections at the boundaries and the chaotic seismic facies towards the inner zone. (D) Close-up of a Type 2 reflection, which typically offset Top Basement and are often associated with an anticline. (E) Close-up of a Type 3 reflection. Note the flat-lying reflections above Top Basement.

Fig. 5. Seismic attributes and interpreted intra-basement reflections in the shallow crystalline basement. (A) Root Mean Square (RMS) Amplitude and (B) Dip Illumination on time slice 2871 ms (see Fig. 2A). Note the high-amplitude zone corresponding to the Type 1 reflections in (A). (C) Interpreted intra-basement reflections based on the maps of RMS Amplitude (A) and Dip Illumination (B). The inset rose diagram highlights the orientation of the intra-basement reflections; note that the strike varies from NNW-SSE to NNE-SSW.

Fig. 6. (A) TWT-structure map of Top Basement. (B) Line drawing of the structures at Top Basement level based on the Top Basement map in (A). (C) Map showing Top Basement structures (in black) together with the intra-basement reflections interpreted on time-slice 2871 ms (in grey). Note the plan-view correlation between Top Basement reverse structures and intra-basement reflections.

Fig. 7. TWT-structure maps and line drawing illustrating the structural style at different levels of the sedimentary cover (see Fig. 2A). (A) TWT-structure map of Top Tikorangi Formation and (B) line drawing of the interpreted structures. Grey lines delineate the underlying Top Basement structures. Note the plan-view correlation between Top Basement reverse structures and later rift-related faults. (C) TWT-structure map of the Intra-Giant Foresets Formation Horizon and (D) line drawing of the interpreted structures. The mean fault strike highlighted by the inset rose diagram is NNE-SSW. (E) Map showing the normal faults on Intra-Giant Foresets Formation Horizon (coloured segments) together with the underlying intra-basement structures (in grey) in the northern part of the survey (location shown in Fig. 7D). Note the plan-view correlation between the Type 1 structure and the overlying normal faults.

Fig. 8. TWT-thickness maps of the stratigraphic intervals corresponding to the rifting events of the Taranaki Basin (see Fig. 2A). (A) Top Basement - Top Farewell Formation interval (Paleocene). The red box indicates a local thickness decrease corresponding to the edge of the underlying Type 1 structure. (B) Top Upper Manganui Formation - Intra-Giant Foresets Formation Horizon interval (pre-Pliocene rifting). (C) Intra-Giant Foresets Formation Horizon – Top Giant Foresets Formation interval (Pliocene rifting). Note that across-fault thickness variations are only observed in (C). The location of the maps is shown in Fig. 7D.

Fig. 9. Quantitative analysis of faults F1 and F2. (A) Throw distribution on faults F1 and F2. Each fault surface displays a single throw maximum, with broadly elliptical contours. Dashed lines indicate the intersection of the fault planes with the seismic section and the map shown in Figs. 9B and E, respectively. The grey surface is Top Basement. (B) Seismic section oriented orthogonal to F1 and F2 (location shown in Fig. 9E). Note the straight, steep (60°) fault surfaces and the presence of a Type 2 structure under the cover faults. (C) T-z and (D) expansion index plots taken from the seismic section in (B). Note the broadly, symmetrical throw profiles. (E) Simplified map based on Top Tikorangi Formation showing the location of F1, F2 and the other normal faults disconnected from intra-basement structures (in red).

Fig. 10. Quantitative analysis of F3, F4 and F5. (A) Throw distribution on F3-F5. Each fault displays a single throw maximum, and negative throw values near Top Basement. Dashed lines indicate the intersection of the fault planes with the seismic section and the map shown in Figs. 10B and E, respectively. The grey surface is Top Basement. (B) Seismic section oriented orthogonal to F3 (location shown in Fig. 10E). Note the physical linkage between F3 and the underlying Type 2 structure. (C) T-z and (D) expansion index plots taken from the seismic section in (B). Note the rapid transition from negative to positive throw values near Top Basement. (E) Simplified map based on Top Tikorangi Formation showing the location of F3, F5, and the other NW-SE-striking normal faults physically connected to Type 2 structures (in red).

Fig. 11. Quantitative analysis of F6a and F6b. (A) Throw distribution on F6a and b. The fault segments are physically connected along a small portion of their length, and display two distinct throw maxima. Dashed lines indicate the intersection of the fault planes with the seismic section and the map shown in Figs. 11B and E, respectively. The grey surface is Top

Basement. (B) Seismic section oriented orthogonal to F6a and b (location shown in Fig. 11E). Note the physical linkage between F6a and the underlying Type 2 structure. (C) T-z and (D) expansion index plots taken from the seismic section in (B). (E) Simplified map based on Top Tikorangi Formation showing the location of F6a, b and the other NE-SW to NNE-SSW-striking normal faults physically connected to Type 2 structures (in red).

Fig. 12. Quantitative analysis of F7. (A) Throw distribution on F7. The fault plane splays upwards into three, en-echelon, left-stepping segments, having discrete throw maxima (F7a, F7b and F7c). A fourth, elongated throw maximum is present on the lower part of the fault. Dashed lines indicate intersection of the fault planes with the seismic section and the maps shown in Figs. 12B, E and F. (B) Seismic section oriented orthogonal to F7 (location shown in Fig. 12E). Note the sigmoidal cross-sectional geometry of the fault surface, and physical connection with the underlying Type 1 structure. (C) T-z and (D) expansion index plots taken from the seismic section in (B). Note the B-shaped profile and the negative throw values near Top Basement. (E) Simplified map based on Top Tikorangi Formation showing the location of F7 and the other normal faults physically connected to the Type 1 structure (in red). (F) Simplified map based on Intra-Giant Foresets Formation horizon. Note the presence of three distinct fault segments at this stratigraphic level (F7a, b and c; in red).

Fig. 13. Synoptic figure illustrating the structural evolution of the study area. Block diagrams have been cut along horizontal sections to highlight the possible geometric relationships between structures at different levels. (A)-(B) Note the selective reactivation and upward propagation of intra-basement structures during late Miocene inversion. (C) Pre-existing structures offered sites for the nucleation of new normal faults and locally perturb the regional stress field during Plio-Pleistocene rifting. Note that type, strike and reactivation

history of intra-basement structures determine whether, and to which extent, they influence overlying normal faults, producing different geometric and kinematic relationships (cf. case 1, 2 and 3).

Figures

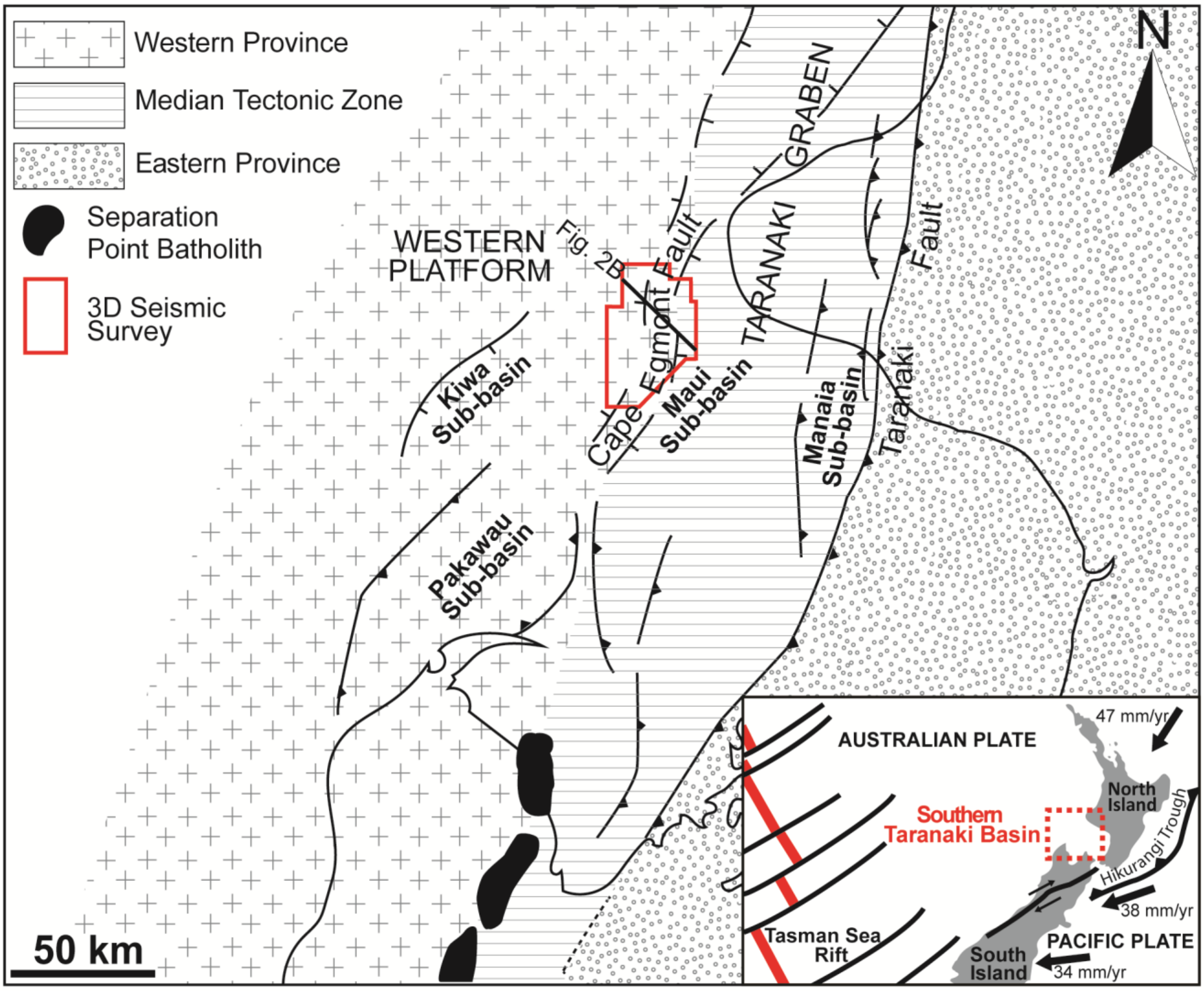

Fig. 1

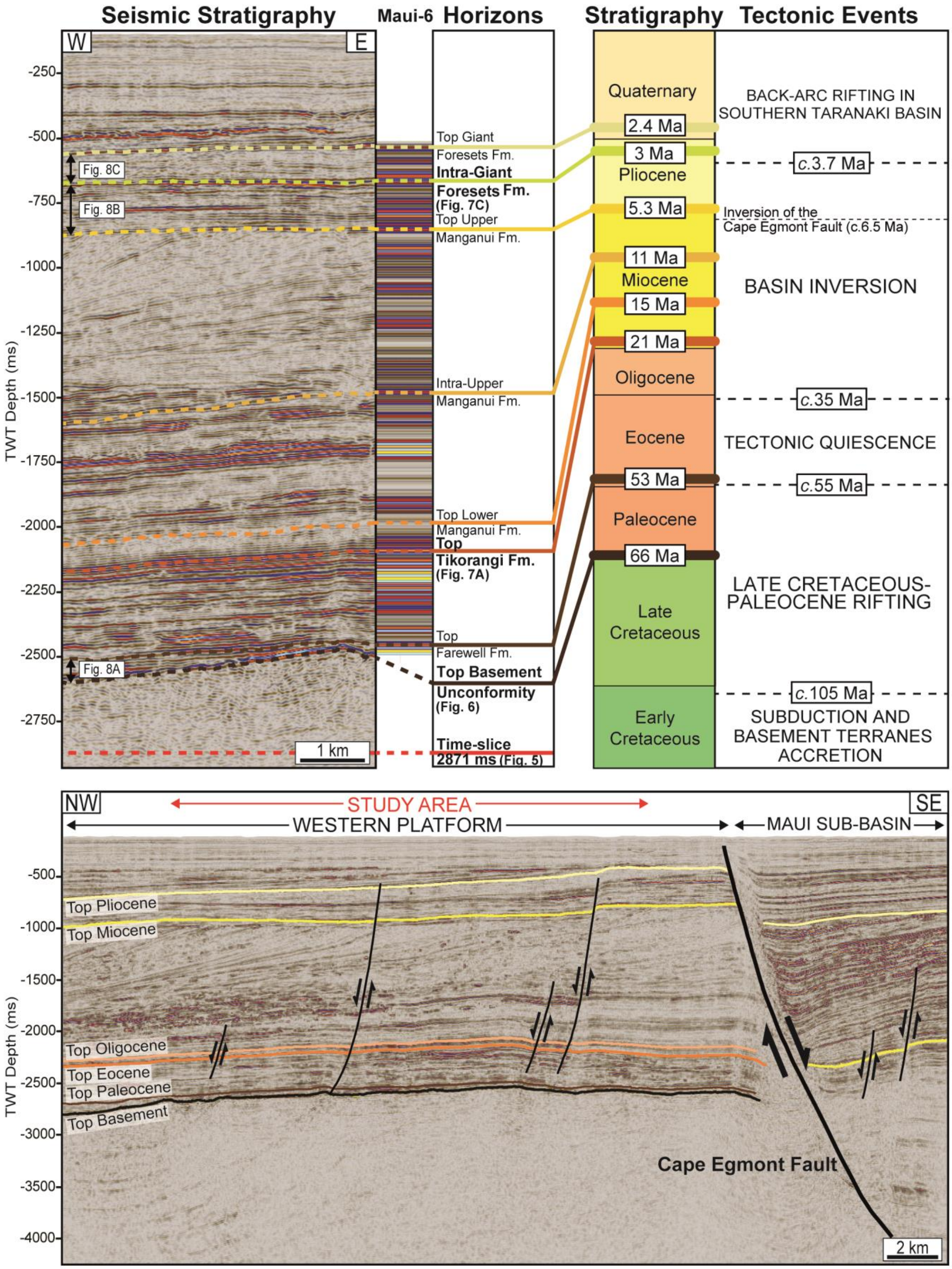
Seismic Stratigraphy
W
E
Maui-6
Horizons
Stratigraphy
Tectonic Events
TWT Depth (ms)
Fig. 8C
Fig. 8B
Fig. 8A
1 km
Top Giant Foresets Fm.
Intra-Giant Foresets Fm. (Fig. 7C)
Top Upper Manganui Fm.
Intra-Upper Manganui Fm.
Top Lower Manganui Fm.
Top Tikorangi Fm. (Fig. 7A)
Top Farewell Fm.
Top Basement Unconformity (Fig. 6)
Time-slice 2871 ms (Fig. 5)
Quaternary
2.4 Ma
3 Ma
Pliocene
5.3 Ma
11 Ma
Miocene
15 Ma
21 Ma
Oligocene
Eocene
53 Ma
Paleocene
66 Ma
Late Cretaceous
Early Cretaceous
BACK-ARC RIFTING IN SOUTHERN TARANAKI BASIN
c.3.7 Ma
Inversion of the Cape Egmont Fault (c.6.5 Ma)
BASIN INVERSION
c.35 Ma
TECTONIC QUIESCENCE
c.55 Ma
LATE CRETACEOUS-PALEOCENE RIFTING
c.105 Ma
SUBDUCTION AND BASEMENT TERRANES ACCRETION
NW
SE
STUDY AREA
WESTERN PLATFORM
MAUI SUB-BASIN
Top Pliocene
Top Miocene
Top Oligocene
Top Eocene
Top Paleocene
Top Basement
Cape Egmont Fault
2 km

Fig. 2

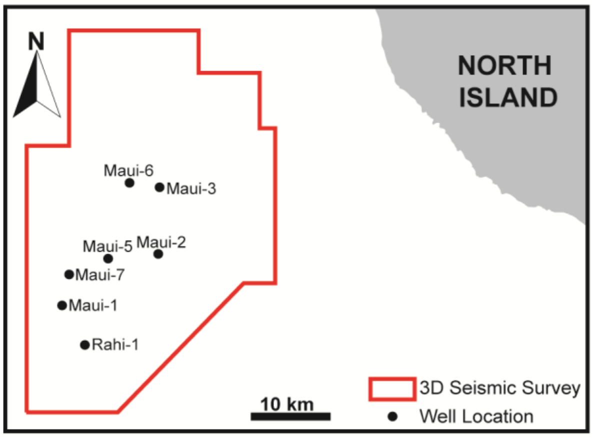
N
NORTH
ISLAND
Maui-6
Maui-3
Maui-5
Maui-2
Maui-7
Maui-1
Rahi-1
10 km
3D Seismic Survey
Well Location

Fig. 3

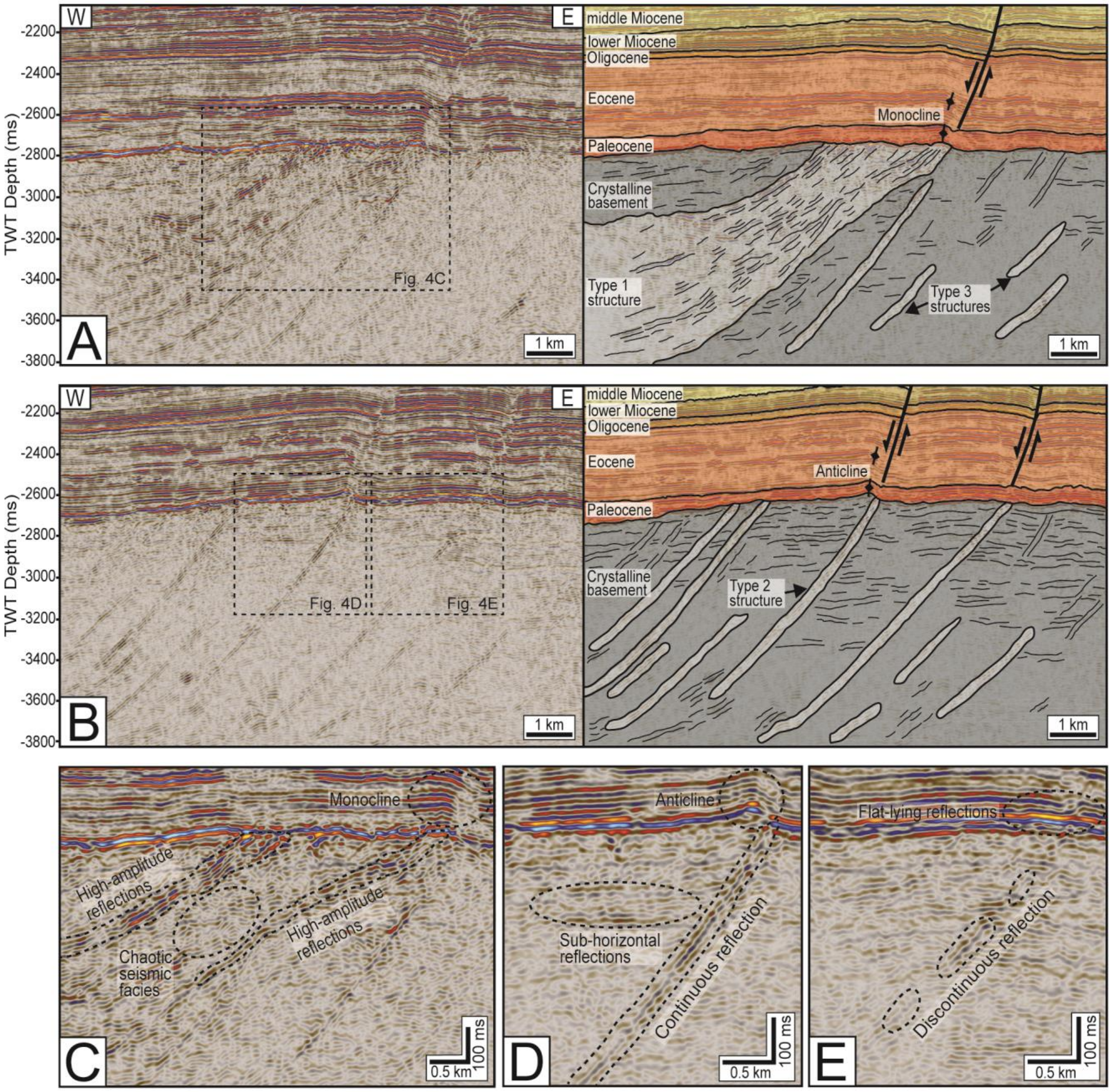

W
E
TWT Depth (ms)
-2200
-2400
-2600
-2800
-3000
-3200
-3400
-3600
-3800
Fig. 4C
A
1 km
middle Miocene
lower Miocene
Oligocene
Eocene
Monocline
Paleocene
Crystalline basement
Type 1 structure
Type 3 structures
Fig. 4D
Fig. 4E
B
Anticline
Type 2 structure
Monocline
High-amplitude reflections
Chaotic seismic facies
C
0.5 km
100 ms
Sub-horizontal reflections
Continuous reflection
D
Flat-lying reflections
Discontinuous reflection
E

Fig. 4

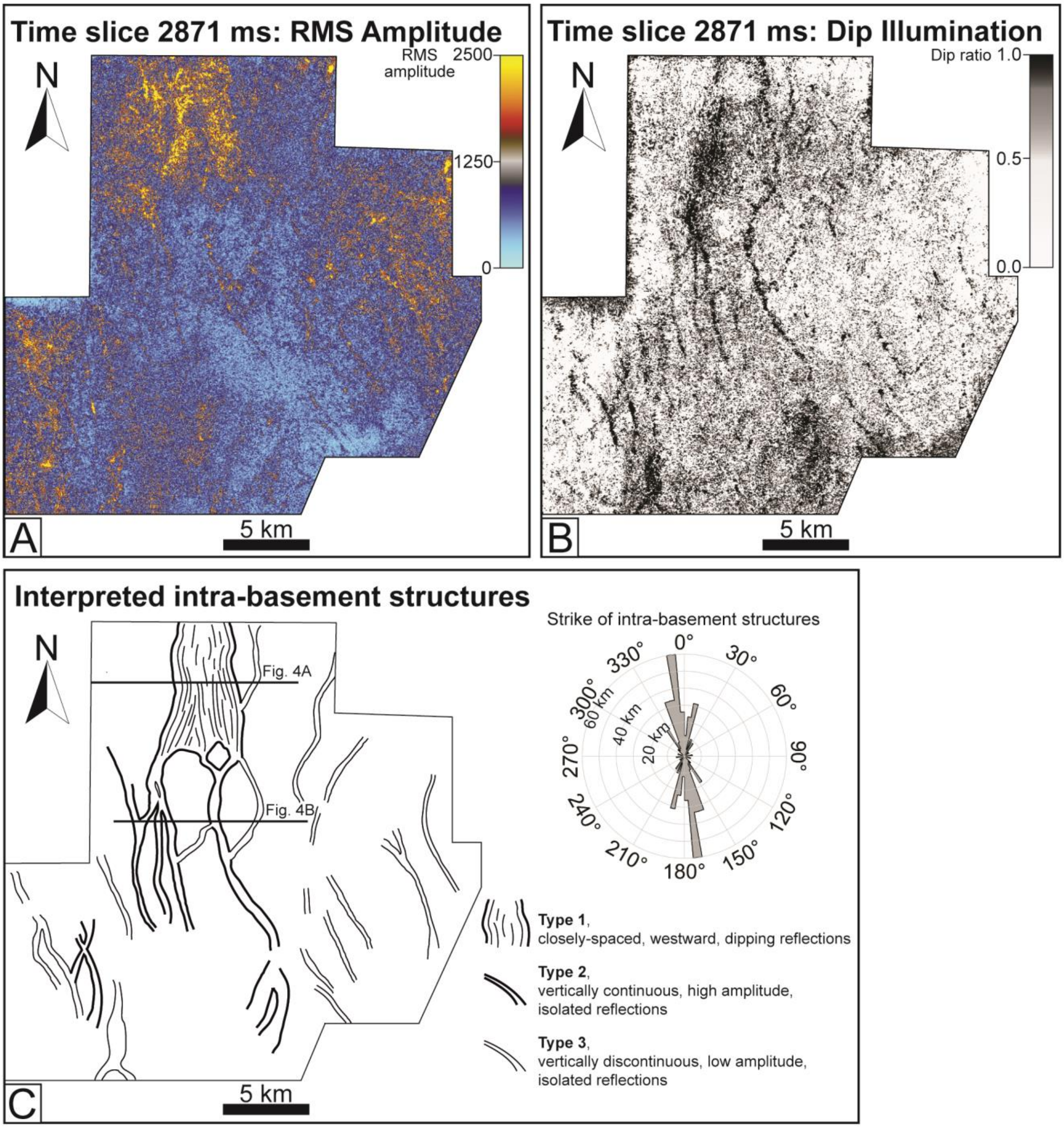

1067

1068 Fig. 5

1069

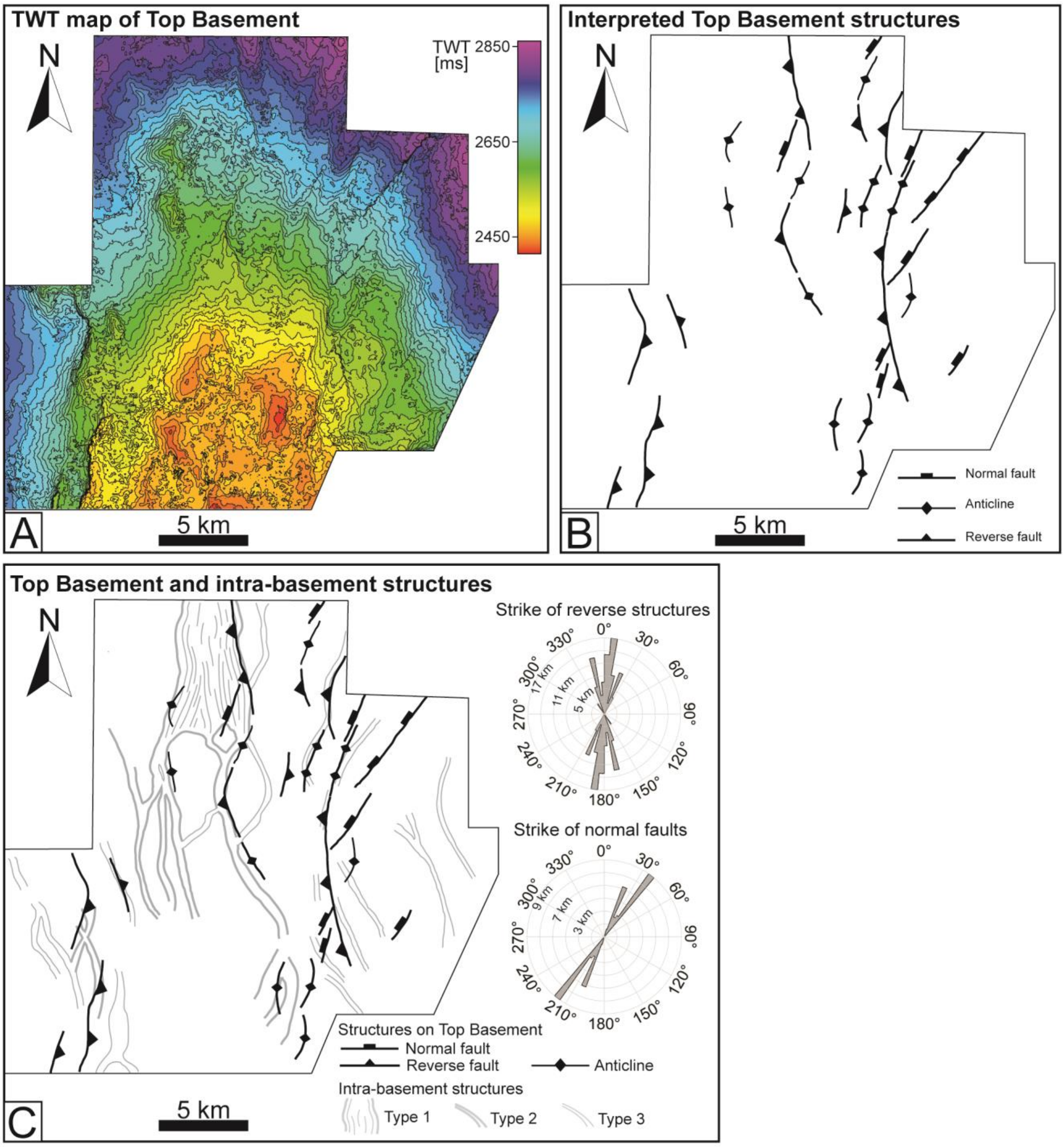
TWT map of Top Basement
N
TWT [ms]
2850
2650
2450
A
5 km
Interpreted Top Basement structures
N
Normal fault
Anticline
Reverse fault
B
5 km
Top Basement and intra-basement structures
N
Strike of reverse structures
0°
30°
60°
90°
120°
150°
180°
210°
240°
270°
300°
330°
17 km
11 km
5 km
Strike of normal faults
0°
30°
60°
90°
120°
150°
180°
210°
240°
270°
300°
330°
9 km
7 km
3 km
Structures on Top Basement
Normal fault
Reverse fault
Anticline
Intra-basement structures
Type 1
Type 2
Type 3
C
5 km

Fig. 6

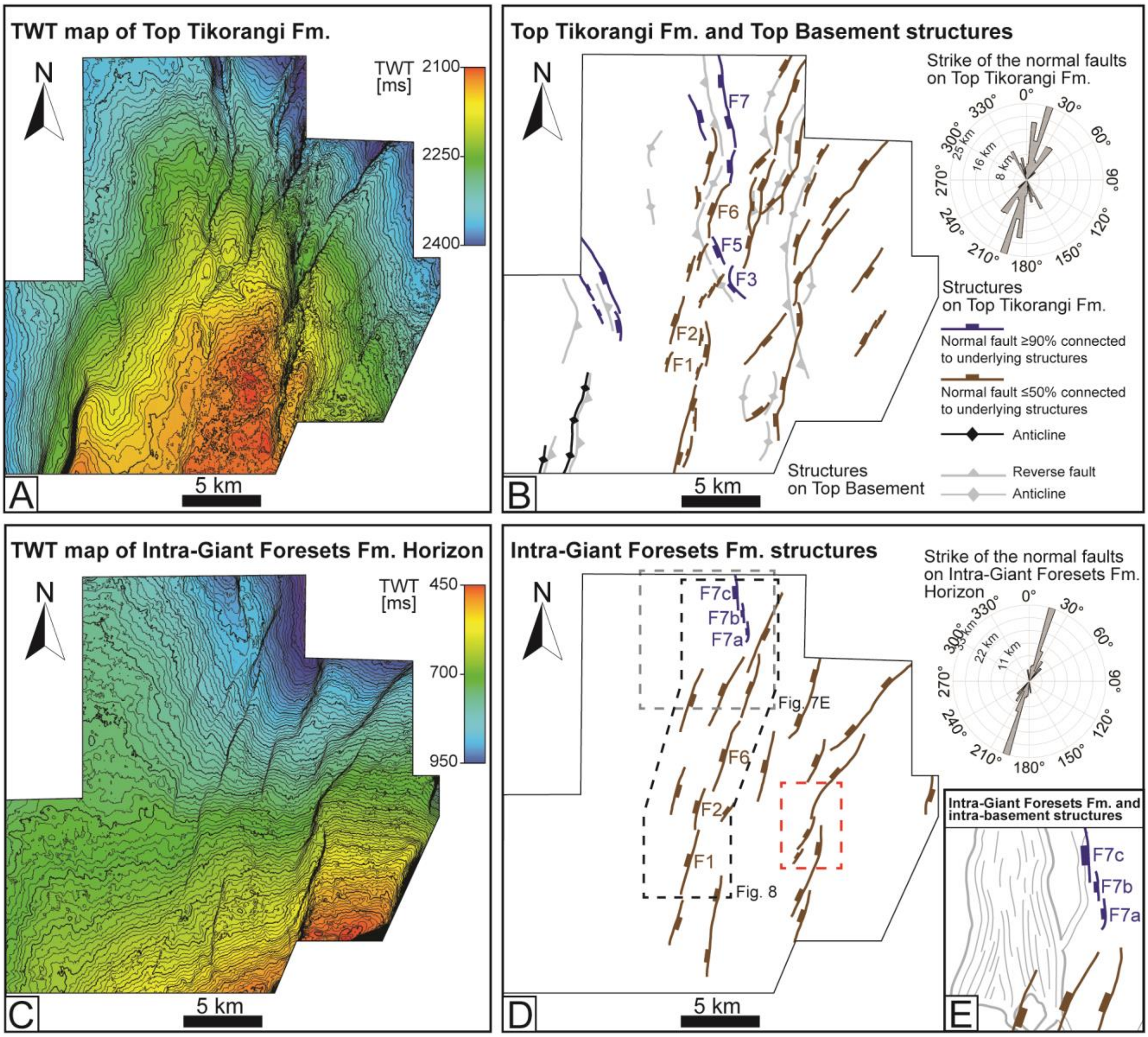
TWT map of Top Tikorangi Fm.
N
TWT [ms]
2100
2250
2400
5 km
A
Top Tikorangi Fm. and Top Basement structures
F7
F6
F5
F3
F2
F1
Strike of the normal faults on Top Tikorangi Fm.
0°
30°
60°
90°
120°
150°
180°
210°
240°
270°
300°
330°
25 km
16 km
8 km
Structures on Top Tikorangi Fm.
Normal fault ≥90% connected to underlying structures
Normal fault ≤50% connected to underlying structures
Anticline
Structures on Top Basement
Reverse fault
Anticline
B
TWT map of Intra-Giant Foresets Fm. Horizon
TWT [ms]
450
700
950
C
Intra-Giant Foresets Fm. structures
F7c
F7b
F7a
Fig. 7E
Fig. 8
Strike of the normal faults on Intra-Giant Foresets Fm. Horizon
33 km
22 km
11 km
D
Intra-Giant Foresets Fm. and intra-basement structures
E

Fig. 7

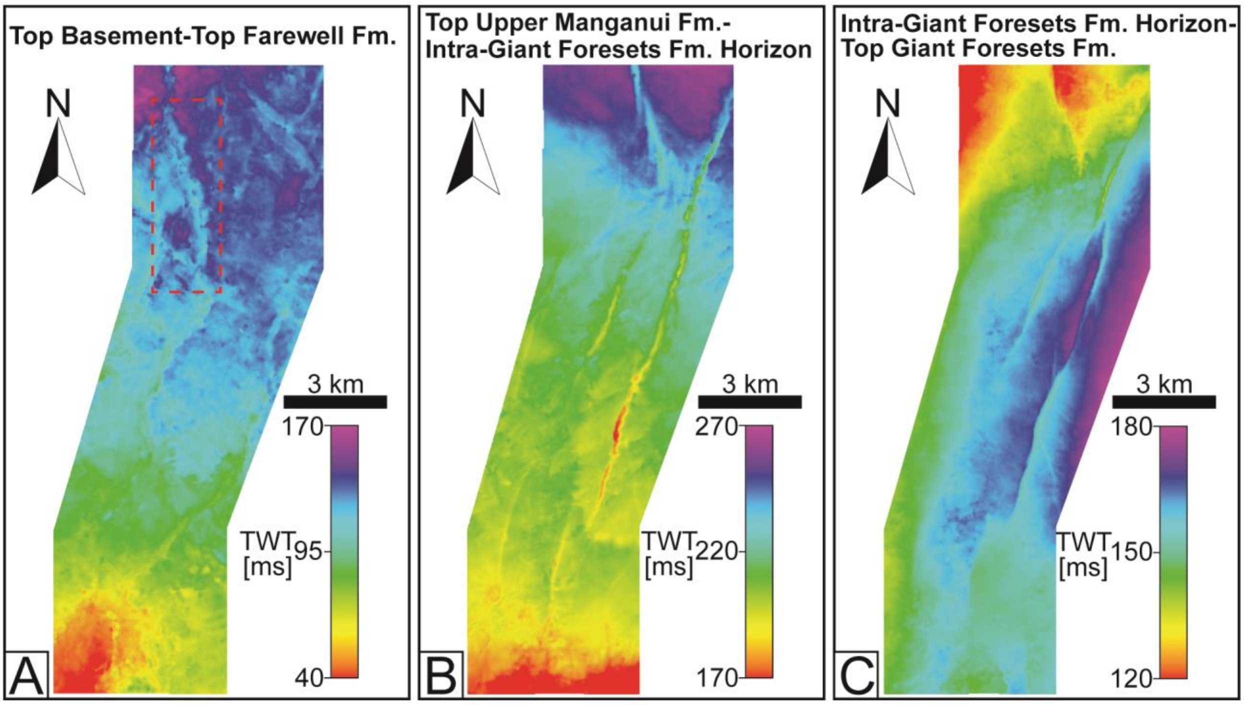
Top Basement-Top Farewell Fm.
Top Upper Manganui Fm.-
Intra-Giant Foresets Fm. Horizon
Intra-Giant Foresets Fm. Horizon-
Top Giant Foresets Fm.
N
3 km
TWT
[ms]
170
95
40
270
220
170
180
150
120
A
B
C

Fig. 8

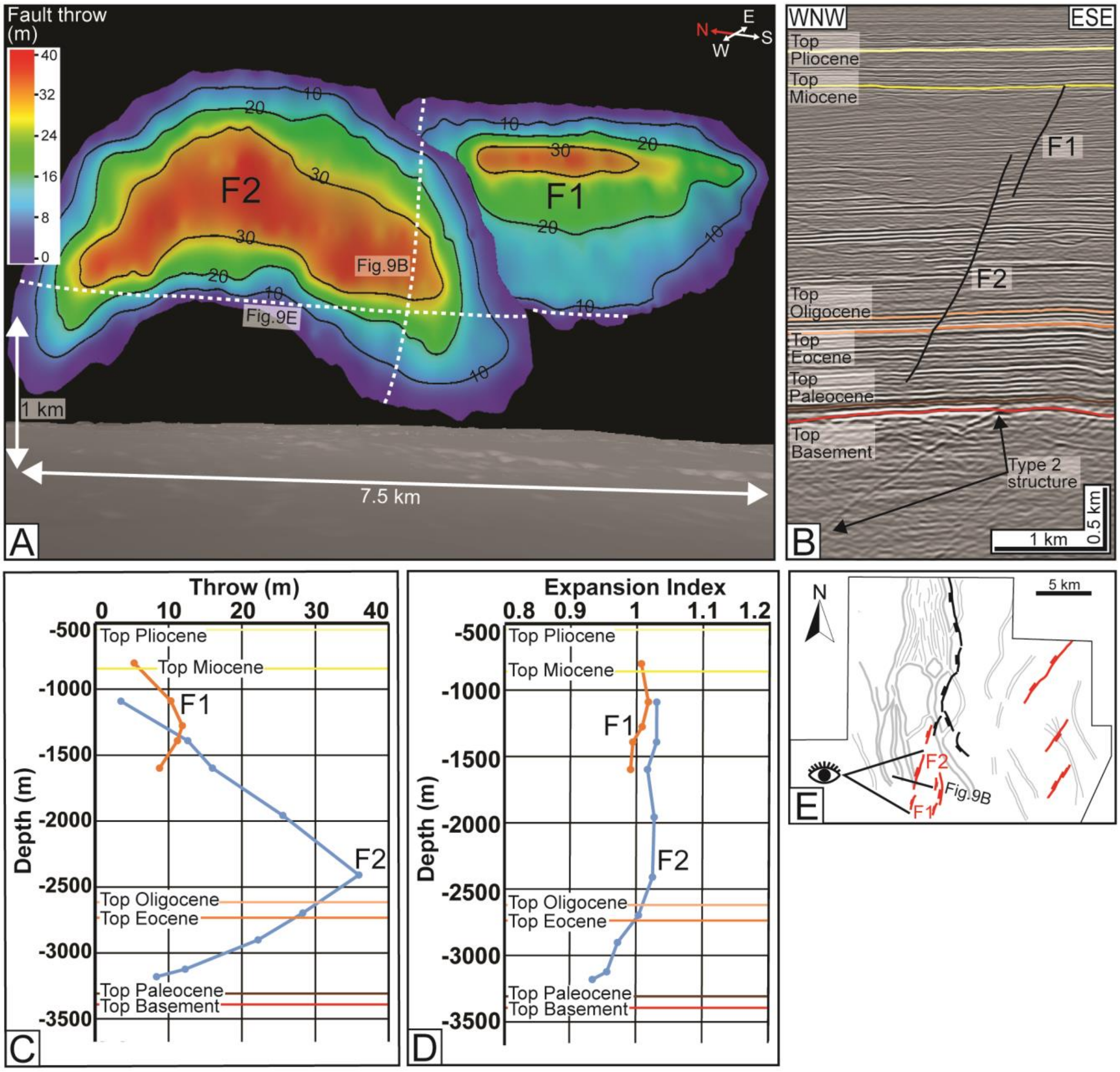
Fault throw (m)
40
32
24
16
8
0
N
E
W
S
F2
F1
10
20
30
Fig.9B
Fig.9E
1 km
7.5 km
A
WNW
ESE
Top Pliocene
Top Miocene
F1
F2
Top Oligocene
Top Eocene
Top Paleocene
Top Basement
Type 2 structure
0.5 km
1 km
B
Throw (m)
0
10
20
30
40
Depth (m)
-500
-1000
-1500
-2000
-2500
-3000
-3500
Top Pliocene
Top Miocene
F1
F2
Top Oligocene
Top Eocene
Top Paleocene
Top Basement
C
Expansion Index
0.8
0.9
1
1.1
1.2
Depth (m)
-500
-1000
-1500
-2000
-2500
-3000
-3500
Top Pliocene
Top Miocene
F1
F2
Top Oligocene
Top Eocene
Top Paleocene
Top Basement
D
N
5 km
F2
Fig.9B
F1
E

Fig. 9

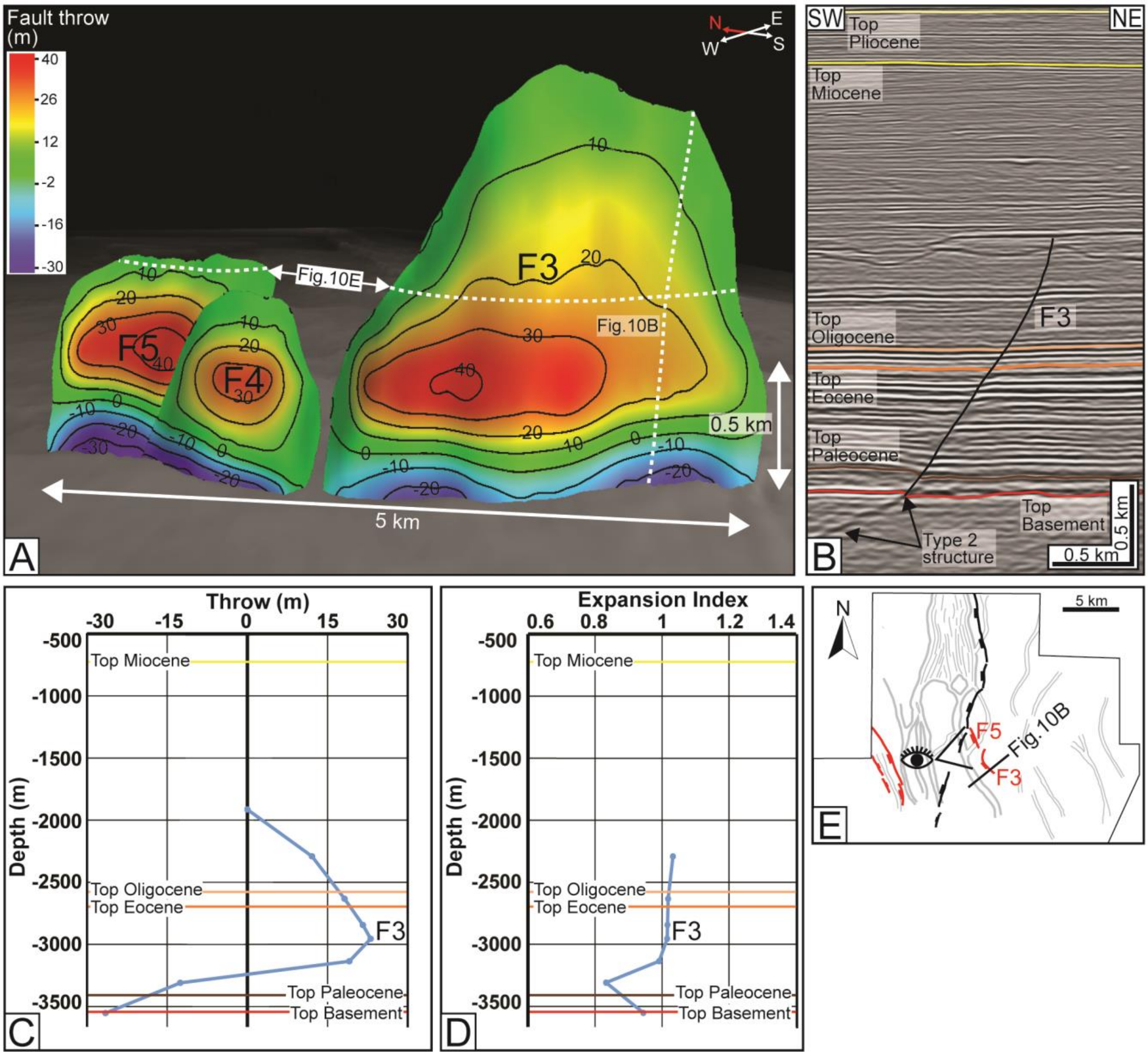

Fault throw (m)
40
26
12
-2
-16
-30
N
E
W
S
F5
F4
F3
Fig.10E
Fig.10B
0.5 km
5 km
A
SW
NE
Top Pliocene
Top Miocene
Top Oligocene
Top Eocene
Top Paleocene
Top Basement
F3
Type 2 structure
0.5 km
0.5 km
B
Throw (m)
-30
-15
0
15
30
Depth (m)
-500
-1000
-1500
-2000
-2500
-3000
-3500
Top Miocene
Top Oligocene
Top Eocene
F3
Top Paleocene
Top Basement
C
Expansion Index
0.6
0.8
1
1.2
1.4
Depth (m)
Top Miocene
Top Oligocene
Top Eocene
F3
Top Paleocene
Top Basement
D
N
5 km
F5
F3
Fig.10B
E

Fig. 10

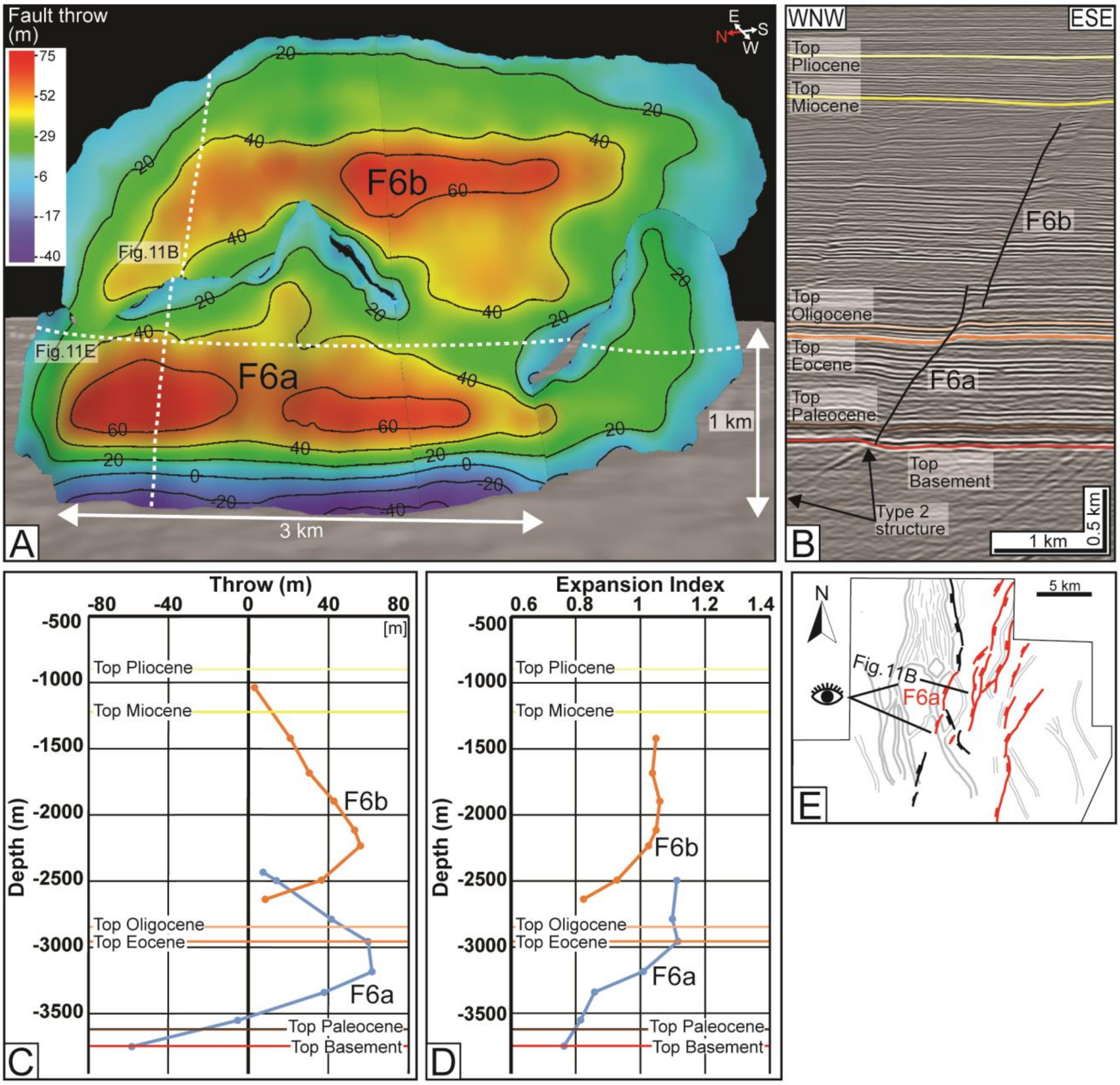
Fault throw (m)
75
52
29
6
-17
-40
E
S
N
W
F6b
F6a
Fig.11B
Fig.11E
1 km
3 km
A
WNW
ESE
Top Pliocene
Top Miocene
F6b
Top Oligocene
Top Eocene
F6a
Top Paleocene
Top Basement
Type 2 structure
0.5 km
1 km
B
Throw (m)
Depth (m)
Top Pliocene
Top Miocene
F6b
Top Oligocene
Top Eocene
F6a
Top Paleocene
Top Basement
C
Expansion Index
Depth (m)
D
N
5 km
Fig. 11B
F6a
E

Fig. 11

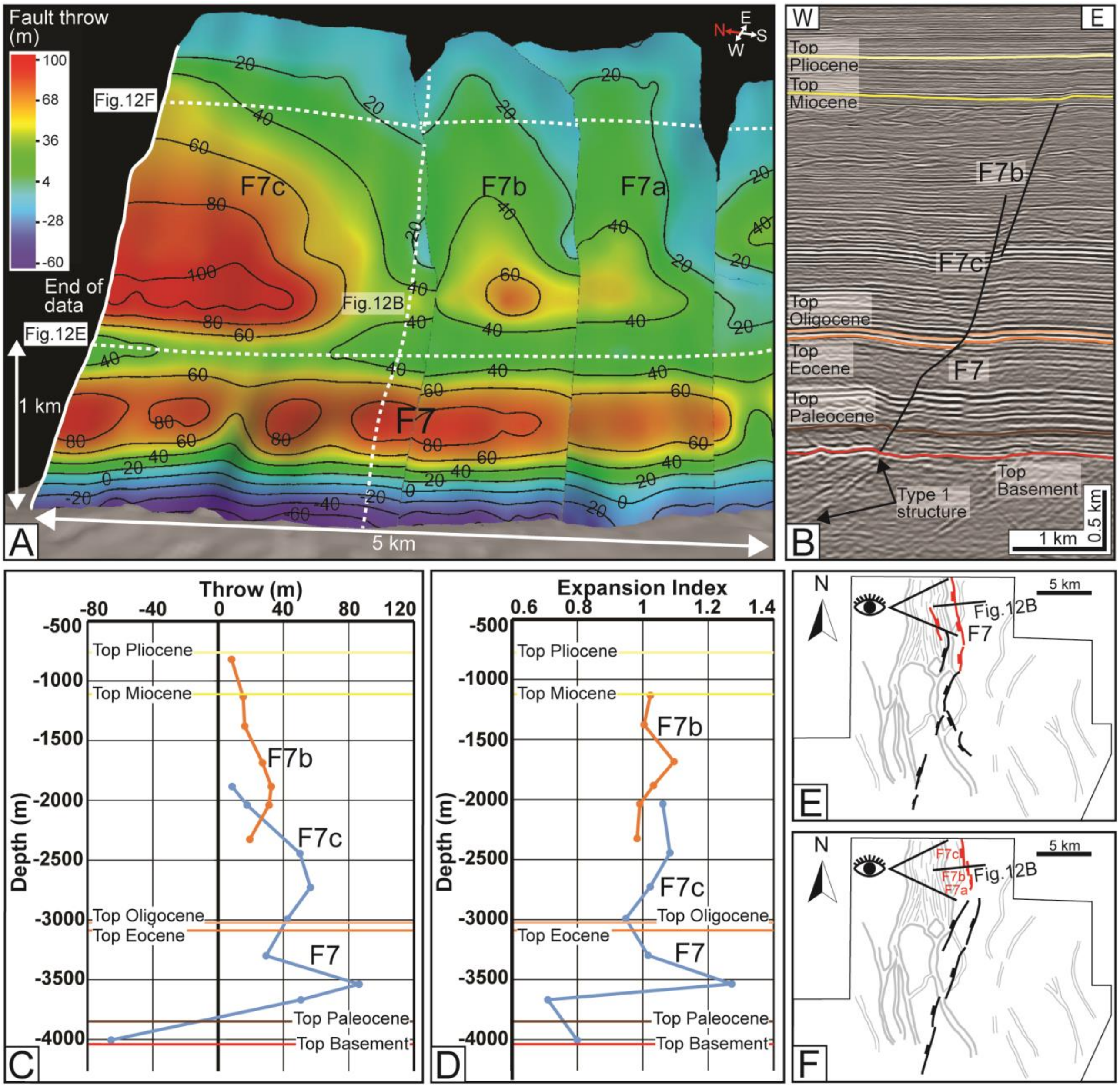
Fault throw (m)
100
68
36
4
-28
-60
N
E
W
S
Fig.12F
Fig.12B
Fig.12E
End of data
F7c
F7b
F7a
F7
1 km
5 km
A
W
E
Top Pliocene
Top Miocene
Top Oligocene
Top Eocene
Top Paleocene
Top Basement
Type 1 structure
1 km
0.5 km
B
Throw (m)
-80 -40 0 40 80 120
Depth (m)
-500
-1000
-1500
-2000
-2500
-3000
-3500
-4000
C
Expansion Index
0.6 0.8 1 1.2 1.4
D
5 km
E
F

Fig. 12

1091 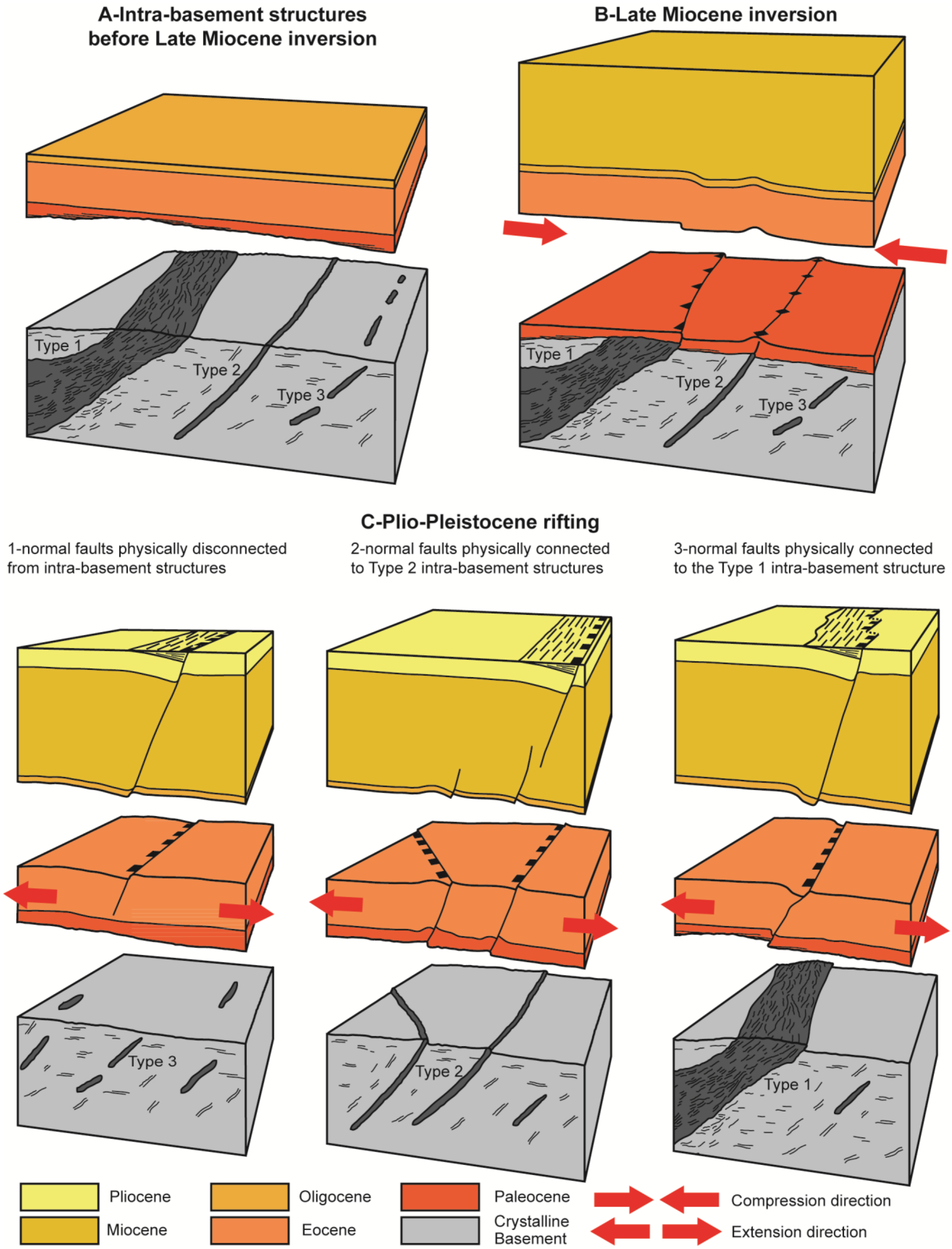

1092 Fig. 13